Journal for ImmunoTherapy of Cancer

The NR_109/FUBP1/c-Myc axis regulates TAM polarization and remodels the tumor microenvironment to promote cancer development

Cong Zhang [1,2] Sisi Wei,[1,2] Suli Dai,[1,2] Xiaoya Li,[1,2] Huixia Wang,[1,2] Hongtao Zhang,[3] Guogui Sun,[4] Baoen Shan,[1,2] Lianmei Zhao[1,2]

Correspondence to
Professor Lianmei Zhao;
zhaolianmei@hbydsy.com

ABSTRACT

Background Tumor-associated macrophages (TAMs) are a major component of the tumor microenvironment (TME) and exert an important role in tumor progression. Due to the heterogeneity and plasticity of TAMs, modulating the polarization states of TAMs is considered as a potential therapeutic strategy for tumors. Long noncoding RNAs (lncRNAs) have been implicated in various physiological and pathological processes, yet the underlying mechanism on how lncRNAs manipulate the polarization states of TAMs is still unclear and remains to be further investigated.

Methods Microarray analyses were employed to characterize the lncRNA profile involved in THP-1-induced M0, M1 and M2-like macrophage. Among those differentially expressed lncRNAs, NR_109 was further studied, for its function in M2-like macrophage polarization and the effects of the condition medium or macrophages mediated by NR_109 on tumor proliferation, metastasis and TME remodeling both in vitro and in vivo. Moreover, we revealed how NR_109 interacted with far upstream element-binding protein 1 (FUBP1) to regulate the protein stability through hindering ubiquitination modification by competitively binding with JVT-1. Finally, we examined sections of tumor patients to probe the correlation among the expression of NR_109 and related proteins, showing the clinical significance of NR_109.

Results We found that lncRNA NR_109 was highly expressed in M2-like macrophages. Knockdown NR_109 impeded IL-4 induced M2-like macrophage polarization and significantly reduced the activity of M2-like macrophages to support the proliferation and metastasis of tumor cells in vitro and in vivo. Mechanistically, NR_109 competed with JVT-1 to bind FUBP1 at its C-terminus domain, impeded the ubiquitin-mediated degradation of FUBP1, activated *c-Myc* transcription and thus promoted M2-like macrophages polarization. Meanwhile, as a transcription factor, c-Myc could bind to the promoter of NR_109 and enhance the transcription of NR_109. Clinically, high NR_109 expression was found in CD163^{+} TAMs from tumor tissues and was positively correlated with poor clinical stages of patients with gastric cancer and breast cancer.

Conclusions Our work revealed for the first time that NR_109 exerted a crucial role in regulating the phenotype-remodeling and function of M2-like macrophages via

WHAT IS ALREADY KNOWN ON THIS TOPIC

⇒ As a heterogeneous and plastic population of cells, switching macrophages from a protumor state to an antitumor phenotype is a promising strategy for cancer immunotherapy. Previous studies have shown that lncRNAs are involved in remodeling macrophage polarization, yet the detailed mechanism remains elusive.

WHAT THIS STUDY ADDS

⇒ In our work, we identified for the first time that lncRNA NR_109 facilitated the M2-like macrophage polarization via a NR_109/far upstream element-binding protein 1/c-Myc positive feedback loop and further promoted tumor progression.

HOW THIS STUDY MIGHT AFFECT RESEARCH, PRACTICE OR POLICY

⇒ Our findings revealed the role of NR_109 in regulating M2-like macrophage polarization and had great translation potentials in the diagnosis, prognosis and immunotherapy of cancer.

a NR_109/FUBP1/c-Myc positive feedback loop. Thus, NR_109 has great translational potentials in the diagnosis, prognosis and immunotherapy of cancer.

BACKGROUND

Contributing to tumorigenesis and tumor development, the tumor microenvironment (TME) contains a complex profile of cells, cytokines and chemokines.[1 2] As a major component of immune cells in the TME, tumor-associated macrophages (TAMs) account for up to 50% of cells in the tumor mass and are generally relevant to worse prognosis in cancer patients.[3 4] Macrophages have traditionally been divided into the antitumor M1-like phenotype which has high levels of iNOS, TNF-α or IL-12 and the pro-tumor M2-like phenotype, which is characterized by high expression of Arg-1, CD206, IL-10 or TGF-β.[5] However, this is far from enough

because these two states are not separated entirely but a dynamic process of mutual transformation. With recent single-cell analysis using mass spectrometric and RNA sequencing techniques, a new dimension has been added to the dissection of macrophage diversity.[6 7] Although the concept of M1-like and M2-like macrophage is no longer considered appropriate, most studies continue to use M1-M2 associated markers for characterization of TAMs, as there is extensive experience based on the correlation between their expression and prognosis in tumor models and human cancers.[8–10]

TAMs usually exhibit the properties of M2-like macrophages in TME and are involved directly or indirectly in tumor progression.[11–13] As TAMs are a dynamic population of cells, switching TAMs toward an antitumor phenotype may provide an opportunity to reshape the immunosuppressive TME and restrain the development of cancers. Despite recent progress in preclinical and clinical studies, there are still some unanswered questions. Thus, illustrating the exact mechanisms of macrophage polarization could help explore promising and effective immunotherapies for tumors.

Long non-coding RNAs (lncRNAs), mainly localized in the nucleus, are typically longer than 200 nucleotides and have little or no protein-coding potential.[14 15] By interacting with DNA, RNA and proteins, lncRNAs exert their functions via epigenetic modification, transcriptional control and translational regulation, and are linked to the pathogenesis of diseases.[16 17] Recent reports have shown that some lncRNAs participate in macrophage polarization, such as MM2P and RPPH1.[18–20] However, the detailed molecular mechanisms of lncRNAs on macrophage polarization remain to be deeply elucidated.

In this work, we utilized lncRNA specific microarray assays to identify lncRNAs differentially expressed in M0, M1-like and M2-like macrophages derived from THP-1 cells.[21–23] For the first time, we revealed a novel lncRNA NR_109 which was elevated in M2-like macrophages. Moreover, NR_109 knockdown hindered IL-4 induced M2-like macrophage polarization and transattenuated the proliferation and metastasis of tumors both in vitro and in vivo. Mechanically, NR_109 regulated macrophage phenotype remodeling through a positive feedback loop of NR_109/FUBP1/c-Myc. Overall, our study discovered a novel mechanism on macrophage polarization and provided insights into developing macrophage-targeting cancer immunotherapy.

METHODS
Cell culture
THP-1 human mononuclear cell line, Eca-109 human esophageal cancer cell line, AGS and BGC-823 human gastric cancer (GC) cell lines, MDA-MB-231 human breast cancer cell line and A549 human lung cancer cell line were obtained from the Type Culture Collection of the Chinese Academy of Sciences (Shanghai, China) between 2012 and 2015 and were stored in liquid nitrogen tanks

in the Research Center of the Fourth Hospital of Hebei Medical University. The cells were cultured in RPMI 1640 or DMEM media (both from Gibico, USA) supplemented with 10% fetal bovine serum (FBS), BI, Israel) and maintained at 37°C in a 5% CO_2 incubator. The cell lines used for experiments had been passaged no more than 20 times and cells were monitored for mycoplasma contamination every 6 months.

Preparation and simulation of macrophages
THP-1 cells (3×10^5/mL) were seeded in six-well plates and cultured in RPMI 1640 media with PMA (50 ng/mL, Sigma, USA) for 48 hours, which were considered as M0 macrophages. After resting for 24 hours, we added lipopolysaccharides (LPS), 100 ng/mL, Sigma, USA) and IFN-γ (20 ng/mL, Pepro Tech, USA) or IL-4 (20 ng/mL, Pepro Tech, USA) to the M0 cells to induce M1-like or M2-like macrophages. Peripheral blood monocytes (PBMCs) from healthy donors were isolated by Ficoll density gradient centrifugation and $CD14^+$ cells were separated from freshly isolated PBMC with the Human $CD14^+$ microbeads using a MACS system (Miltenyi Biotec, Germany). For differentiation, $CD14^+$ monocytes were cultured for 6 days in the presence of recombinant human granulocyte-macrophage colony-stimulating factor (GM-CSF), 10 ng/mL, Pepro Tech, USA) or M-CSF (25 ng/mL, Pepro Tech, USA). For M1-like macrophage polarization, monocytes treated with GM-CSF for 6 days were then treated with LPS (100 ng/mL) and IFN-γ (20 ng/mL). For M2-like macrophage polarization, monocytes treated with M-CSF for 6 days were then treated with IL-4 (25 ng/mL).

Microarray analysis
Total RNA was extracted from THP-1-induced M0, M1-like and M2-like macrophages using TRIzol reagent (Invitrogen, USA). RNA integrity was verified using an Agilent 2100 bioanalyzer (Agilent, USA). The expression of lncRNAs and mRNAs in M0, M1-like and M2-like macrophages was analyzed using the lncRNA-specific microarrays (the Agilent SBC human lncRNA Microarray V.6.0 (4×180K), which contained 180,000 probes and was performed by Shanghai Biotechnology). LncRNAs were deemed differentially expressed according to the following criteria: fold change ≥2 or ≤ 0.5, and p<0.05.

Patients and healthy donors
Fresh primary GC tissues, the matched adjacent non-neoplastic tissues and human blood samples were collected from the Fourth Hospital of Hebei Medical University between 2017 and 2018. All samples were diagnosed blindly by 2–3 pathologists. The inclusion criteria required that patients had primary gastric adenocarcinoma at stages I–IV, had received surgery as the initial treatment and had complete clinicopathological data.

TAMs isolation from tissues
TAMs isolated from primary GC tissues (pri-GC) or the matched adjacent non-neoplastic tissues (non-GC)

following a published method by Li *et al* with some modifications.[24] Briefly, the tissues were collected immediately after the surgery, minced into small pieces (1–2 mm) and digested with DNase I (Takara, Japan) and collagenase IV (Sigma, USA) for 2 hours at 37°C under constant shaking. The cells were sequentially filtered through a 100-mesh sieve and then centrifuged at 400 g for 10 min. Then, the cells were resuspended in 2 mL RPMI 1640 medium with 1% FBS and cultured in a 37°C incubator. After 1 hour, the adherent cells were considered as macrophages isolated from tissues.

Rapid amplification of cDNA ends assay
To characterize the 5' and 3' ends of NR_109, total RNA extracted from THP-1-induced M2-like macrophages was used to generate rapid amplification of cDNA ends assay (RACE)-ready cDNA, and PCR was performed using a 5' and 3' RACE System for Rapid Amplification of cDNA Ends Kit (Invitrogen, USA). The cDNA ends were amplified with universal and gene specific primers.

Transfection
Small interfering RNA (siRNAs) against NR_109, far upstream element-binding protein 1 (FUBP1), c-Myc were synthesized by GenePharma (China) and all the plasmids were synthesized by GeneChem (China). siRNA or plasmid transfection was performed with Lipofectamine 2000 (Invitrogen, USA) or NEOFECT DNA transfection reagent (NEOFECT, China), respectively, according to the manufacturers' instructions. Cells were harvested 24–72 hours post-transfection for subsequent analysis. The individual siRNA sequences are listed in online supplemental table 3.

qRT-PCR
Quantitative Real-time PCR (qRT-PCR) was performed using a SYBR Green PCR Kit (Promega, USA) according to the manufacturer's instructions. Data was collected and analyzed with a Real-Time PCR System (ABI 7500, USA). The primer sequences used for qPCR are listed in online supplemental table 3.

ELISA
Supernatants were harvested 48 hours after cytokine treatments or transfection and used for subsequent IL-12, TNF-α, IL-10 and TGF-β ELISA (Enzyme linked immunosorbent) assays (all the ELISA kits purchased from eBioscience, USA). All experiments were performed according to the manufacturer's instructions.

Cell proliferation assay
The MTS assay was performed according to the manufacturer's instructions to examine the proliferation of tumor cells. Tumor cells (5×10^3) were plated in 96-well plates with 6 replicates/group and cocultured with medium containing 30% supernatant of macrophages in different groups. The cells were incubated for 0, 24, and 48 hours. At each of the desired time points, MTS solution (Promega, USA) was added to each well and incubated for 2 hours in the dark at 37°C, followed by measurement of the absorbance at 492 nm with a microplate reader (Cytation5, BioTek).

EdU incorporation assay
A Cell-Light EdU Apollo488 in Vitro Kit (C10310-3, Ribobio) was used to apply the EdU incorporation assay. 1.5×10^4 tumor cells / well were seeded into 96-well plates and treated with 30% supernatant of M2-like macrophages with different NR_109-expressed for 48 hours. Then, the cells were cultured with EdU reagent (1:1000 dilution) for 2 hrs. Four percent paraformaldehyde was used to fix the cells, and fluorescent dye and Hoechst were used to stain cells. The EdU-positive cells was photographed by the confocal microscope (Nikon, Japan) and counted by the Photoshop software.

Transwell assay
For the transwell assays, tumor cells (1×10^5) were seeded in the upper chamber (24-well insert; 8 µm pore size; Corning Costar, Cambridge, Massachusetts, USA) using 0.2 mL of medium without serum, and macrophages (2×10^5) in different groups was added to the lower chamber as a chemoattractant. After a 15–20 hours incubation, non-migrating cells in the upper surface of the membrane were removed with a cotton swab, and the cells that penetrated the lower surface of the membrane were stained with crystal violet. The number of cells invading the membrane was counted with a microscope in five randomly selected fields. Data were obtained from three independent experiments.

Flow cytometry
For cell-surface molecular analysis, cells were suspended in PBS containing 1% FBS, and then stained with PE-conjugated anti-CD86 (12-0869-42), FITC-conjugated anti-CD206 (MA5-16870), PE-conjugated anti-CD163 (12-1639-42), Mouse IgG2b κ Isotype Control PE (12-4732-81), Mouse IgG1, κ Isotype Control Alexa Fluor 488 (53–4714) (all the antibodies purchased from eBioscience, USA), PE/cyanine 5-conjugated anti-CD11b (E-AB-F1081G, Elabscience, China), PE/cyanine 5 Rat IgG2b, κ Isotype Control (E-AB-F09842G, Elabscience, China), CD4-FITC/CD8-PE/CD3-PerCP (340298), CD3-FITC/CD16+56 PE (340042), Mouse IgG1 PE (349043), Mouse IgG1 FITC (349041), Mouse IgG2a PerCP (349054) (all the antibodies purchased from BD, USA) for 30 min at 4°C. For flow cytometry (FCM) gating, cells were stained with isotype-matched control antibodies or unstained cells and other cells were analyzed according to that fating strategy. Specimens were subsequently analyzed by FCM (Navios, Beckman).

Western blotting assay
Proteins were extracted from the cells with RIPA buffer (Solarbio, China), resolved by SDS-polyacrylamide gels, and then transferred to PVDF membranes (Millipore, USA). The following antibodies were used: anti-c-Myc (Abcam, ab39688, USA), anti-FUBP1 (Proteintech,

24864–1-AP, China), anti-JTV-1 (Proteintech, 10 424-1-AP, China), anti-Ubiquitin (Abcam, ab134953, USA), anti-CD206 (Abcam, ab64693, USA) and anti-SCARB1 (Proteintech, 21 277–1-AP, China). Protein levels were normalized to the endogenous GAPDH control (Proteintech, 10 494–1-AP, China) and all the antibodies were diluted in Antibody Diluent (Absin, abs954). IRDye 800CW Goat anti-Rabbit IgG Secondary Antibody (926-32211, LI-COR, USA) and IRDye 680RD Goat anti-Mouse IgG Secondary Antibody (926-68070, LI-COR, USA) were used as the secondary antibody and the antigen-antibody reaction was visualized by detection with an Odyssey assay (Millipore, Billerica, Massachusetts, USA).

Xenograft tumor formation and metastasis assay in mice model

Male HSC-NPG mice (16 weeks old, hCD45$^+$ ≥50%) were obtained from Vitalstar Biotechnology, Beijing. All of the experimental procedures were performed in accordance with the protocols and ethical regulations approved by the Institutional Animal Care and Use Committee of Hebei Medical University (approval number: 2018088). The mice were randomly divided into three groups (six mice per group). BGC-823 cells were mixed with M0, M2sh-NC and M2sh-NR_109 macrophages at a 3:1 ratio and injected into the right flanks of HSC-NPG mice in different groups. Tumor growth was observed daily and photographs were taken on the 21st day and 30th day by an in vivo imaging system (Berthold, NightOWL II LB983, German). The tumor volumes were calculated ($V=0.5 \times \text{length} \times \text{width}^2$ in mice every 3 days. A month after injection, the tumor tissues, peripheral blood sample, spleen and peritoneum macrophages from different groups were collected, and the proportion of immune cells in mice was determined by FCM and immunohistochemical (IHC). To evaluate the role of M2-like macrophage with NR_109 knockdown on tumor lung metastasis, BGC-823 cells were mixed with M2sh-NC or M2sh-NR_109 macrophages at a 3:1 ratio and injected into the tail vein of nude mice in different groups (n=6). Tumor metastasis was monitored using an in vivo imaging system. The mice were sacrificed after 60 days and the lungs were separated and stained with H&E. All animal experiments were performed at the Animal Laboratory Center of the Fourth Hospital of Hebei Medical University.

RNA Fluorescence in situ hybridization

RNA fluorescence in situ hybridization (FISH) assays were performed using a RiboTM Fluorescent in situ hybridization Kit (Ribobio, China) according to the manufacturer's instructions. NR_109, 18S RNA and U6 probes were labeled with Cy3 fluorescent dye. Briefly, M2-like macrophages were seeded onto sterile slides, fixed with 4% paraformaldehyde and permeabilized with 0.5% Triton X-100 for 30 min. Then, cells were blocked with prehybridization buffer for 30 min at 37°C, followed by incubation in 0.5 µg/mL probe at 37°C for 18 hours. The next day, cells were washed with SSC buffer and stained with DAPI for 10 min. Fluorescence detection was performed with a confocal laser-scanning microscope (A1RHD25, Nikon).

In situ hybridization

The expression of NR_109 in tumor tissues was detected using digoxin-labeled NR_109 in situ hybridization (ISH) probes (BOSTER, China) according to the protocol provided by the manufacturer. Briefly, the formalin fixed paraffin embedded tissue slides were deparaffinized and deproteinated. Slides were then prehybridized in prehybridization solution for 2 hours at 42°C and incubated in DIG-labeled NR_109 probe solution (200 nM) over night at 42°C. The next day, the slides were incubated with anti-DIG reagent, and the probe signal was visualized with diaminobenzidine (DAB) solution followed by counterstaining with hematoxylin. The expression of NR_109 was assessed using the serial sections from the same blocks used for CD68/CD163 IHC staining. For measurement of NR_109 intensity, staining data were captured under a light microscope (magnification×400, Nikon) in five areas per slide and the score was in the range of 1–4 as follows: 1 (no staining), 2 (weak staining), 3 (medium staining), and 4 (strong staining). The scores of 1 and 2 were considered as low expression of NR_109, while the scores of 3 and 4 were considered as high expression of NR_109. Data were analyzed in a double-blinded miner by two pathologists.

Immunofluorescence and IHC staining

First, tissue sections were deparaffinized, rehydrated with graded ethanol, incubated with 0.3% hydrogen peroxide for 20 min, and blocked with goat serum. For immunofluorescence (IF) assay, the slides were incubated with CD206 antibody (Abcam, ab64693) overnight and fluorescent labeled secondary antibodies for 2 hours, IF images were captured by laser confocal microscopy (Nikon, Japan). For IHC (Immunohistochemistry) staining, slides were first incubated overnight with antibodies against Ki67 (dilution 1:5000, Proteintech, 27 309-1-AP), E-cadherin (dilution 1:2000, Proteintech, 20 874-1-AP), Vimentin (dilution 1:2000, Proteintech, 10 366-1-AP), N-cadherin (dilution 1:1000, Proteintech, 22 018-1-AP), CD4 (MXB, RMA-0620), CD8 (MXB, RMA-0514), CD163 (dilution 1:200, Sigma-Aldrich, 163M-14-RUO), CD68 (dilution 1:100, DAKO, M0876), FUBP1 (dilution 1:100, ZENBIO, R24365) and c-Myc (dilution 1:200, Abcam, ab39688) at 4°C and then labeled with a rabbit HRP-conjugated secondary antibody at room temperature for 1 hour. Finally, positive staining was visualized using DAB substrate liquid (Agilent, USA), followed by counterstaining with hematoxylin. All sections were observed and photographed with a microscope (Nikon, Japan). Two pathologists evaluated the IHC scores in a double-blinded manner.

For measurement of the proliferative index, staining data were captured under a light microscope (magnification×400) randomly in five areas per slide. Ki67-positive

cells and cancer cells were counted and the Ki67 index was calculated as Ki67-positive cells/cancer cells. For assessing CD4$^+$ T, CD8$^+$ T and CD163$^+$ cells infiltration in tumor tissues of HSC-NPG mice, three areas with highest infiltration density were used and at least five fields per area were evaluated for markers. The number of stained cells per 20×objective field was counted and converted to cell density (cell number/mm^2). The expression of CD68 or CD163 in human cancer tissues was scored as the percentage of positively stained cells as follows: score 0 (≤10 cells/HP); score 1 (11–29 cells/HP); score 2 (30–49 cells/HP); and score 3 (>50 cells/HP). HP: high-power field, 400×. The expression of FUBP1 and c-Myc in CD68$^+$ cells was scored in a manner consistent with NR_109.

Biotin-RNA pulldown assay
The pGEM-3zf (+)-NR_109 plasmids were linearized by restriction enzyme (Takara, Japan) digestion for use as templates for the transcription of NR_109 sense, antisense and cold probes. Biotin-labeled RNAs were in vitro transcribed using Biotin-RNA Labeling Mix (Roche, Indianapolis, Indiana, USA), treated with RNase-free DNase I (Takara, Kyoto, Japan) and purified with LiCl (Invitrogen, USA). Total protein lysates of M2-like macrophages were mixed with biotinylated RNA and incubated at 30°C. Streptavidin agarose beads (GE Healthcare, Little Chalfont, UK) were added to each binding reaction and further incubated at room temperature with rotation. Complexes of RNA-protein beads were washed with washing buffer and then boiled in 1×loading buffer for 5 min. RNA affinity captures were subjected to 12% SDS-PAGE and visualized by silver staining. Protein bands were excised and identified by in-gel trypsin digestion, followed by mass spectrometry (LC-MS/MS, AB Sciex TripleTOF, ABsciex, Concord, ON, USA).

RNA-immunoprecipitation assay
RNA-immunoprecipitation (RIP) assays were performed using the Magna RIP RNA-Binding Protein Immunoprecipitation kit (Millipore, USA) according to the manufacturer's instructions. Briefly, an antibody directed against FUBP1 was used. The coprecipitated RNAs were adsorbed with magnetic beads (Invitrogen, USA) and detected by RT-PCR. Total RNA (input) and the antibody isotype control rabbit IgG were used simultaneously to demonstrate that the detected signals were from RNAs specifically binding to proteins FUBP1 or others (n=3 for each experiment).

Chromatin immunoprecipitation assay
Chromatin immunoprecipitation (ChIP) was performed using the Magana ChIP A/G Kit (17-10086, Merck, Germany). First, cells were harvested with protein cross-linked to DNA using 1% formaldehyde. Then, chromatin was sheared to lengths of 100–1000 bp using sonication. Next, the sheared and cross-linked chromatin combined with 1–2 μg antibody were used in the immunoprecipitation. c-Myc was employed in the ChIP assay, with goat anti-rabbit IgG used as a negative control. The retrieved DNA was analyzed by agarose gel electrophoresis after PCR. The binding region (BR) primer, forward: GGAAGAATTACAACACTCTTTAGCA, reverse: CAAAAGTCCCAAAGGCATCTAC, the NBR primer, forward: CATCTTGTGCTACCCATTCTATCTT, reverse: GACTAATGGGAGACCTAAAAATACA.

Luciferase reporter assay
Luciferase reporter assays were performed using the Dual-*Luciferase* Reporter Assay System (Promega, USA). Cells were seeded in 24-well plates (1×10^5 cells/well) and transfected with NR_109 plasmids with or without c-Myc BR and *Renilla* plasmids. After 48 hours of transfection, the cells were harvested and analyzed according to the manufacturer's instructions. The luciferase activities were normalized to the *Renilla* luciferase activity of the internal control.

Statistical analysis
Statistical analyses were performed using SPSS V.21.0 software. Data were reported as the mean±SD, unless otherwise noted. Statistical tests for data analysis included Student's t-test, one-way analysis of variance, χ^2-tests, Mann-Whitney U test, Spearman correlation analysis, and Fisher's exact test. All in vitro experiments were repeated with at least three replicates. A p<0.05 was considered statistically significant, and all statistical tests were two sided.

RESULTS
NR_109 was associated with protumor macrophages polarization
To identify the differentially expressed lncRNAs in protumor macrophages, we first set up THP-1-derived models of M0, M1-like and M2-like macrophages according to previous studies.[22 25] As shown in online supplemental figure S1A and B, PMA, LPS/IFN-γ and IL-4 were used to induce macrophages into different phenotypes. Compared with M0 macrophages, the expression of CD86, IL-12, TNF-α, iNOS and HLA-DRα were significantly increased in LPS- and IFN-γ-induced M1-like macrophages, while the expression of CD206, IL-10, TGF-β, Arg-1 and VEGF were elevated in IL-4-treated M2-like macrophages (online supplemental figure S1C–F). All these data confirmed that M1-like and M2-like macrophages derived from THP-1 cells were successfully established.

Subsequently, the SBC Human LncRNA Microarray V.6.0 (4×180 k) (Shanghai Biotechnology, Agilent Microarray Platform) was employed to identify the unique lncRNA and mRNA profiles in M0, M1-like and M2-like macrophages. According to principal component analysis, the M0, M1-like and M2-like macrophages could be distinguished by lncRNAs profiles (figure 1A), highlighting the plausibility and importance of
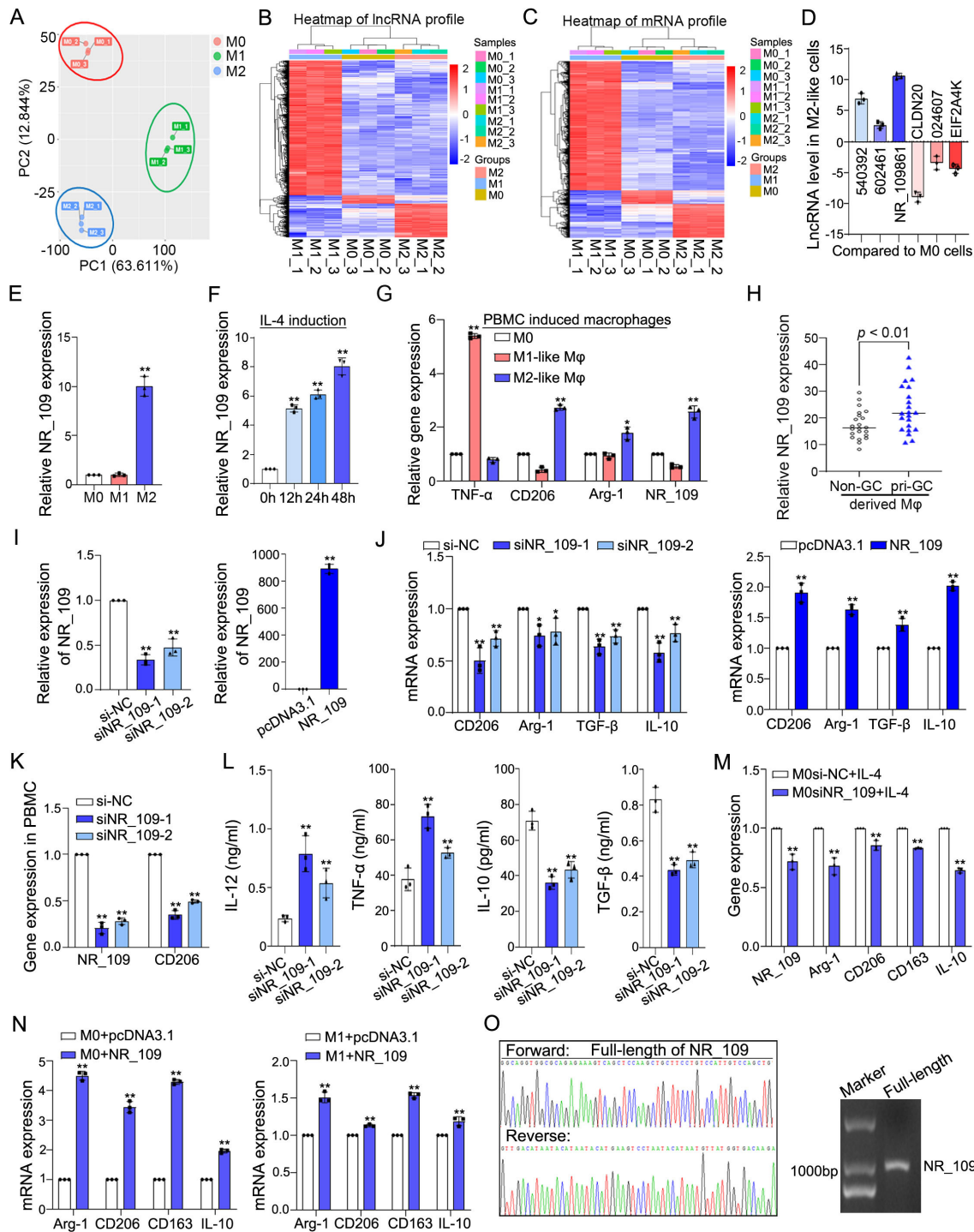
Figure 1 NR_109 was associated with M2-like macrophage polarization. (A) PCA plot from gene expression profiles in M0, M1-like and M2-like macrophages. (B–C). Heatmap of lncRNAs and mRNAs profile in M0, M1-like and M2-like macrophage. (D) Six differentially expressed and immune-related lncRNAs selected from lncRNA microarray data were validated by qPCR. (E) Expression of NR_109 in M0, M1-like and M2-like macrophages was detected by qPCR assays. (F) NR_109 was examined in M0 cells treated with IL-4 for 0, 12, 24 and 48 hours. (G) Expression of NR_109 was analyzed in M2-like macrophages derived from PBMC. (H) Expression of NR_109 in M2-like macrophages derived from primary GC tissues (pri-GC) and the matched adjacent non neoplastic tissues (non-GC) was measured by qPCR. (I) M2-like macrophages with NR_109 knockdown or overexpression were constructed by transfecting with NR_109 siRNA or NR_109 plasmid. (J) Expression of M2-like macrophage markers in IL-4 induced M2-NR_109low cells and M2-NR_109high cells was detected using qPCR. (K) Expression of CD206 was decreased in M2-NR_109low cells derived from PBMC. (L) The level of IL-12, TNF-α, IL-10 and TGF-β in the supernatant of M2-NR_109low cells was analyzed by ELISA. (M) Knockdown NR_109 in M0 cells hindered IL-4 induced M2-like macrophage polarization and the expression of M2-related markers. (N) Expression of M2-related markers in M0 and M1-like macrophages with forced expression of NR_109 were tested by qPCR. (O) RACE assay showed the whole-length of NR_109. The statistical data are from three independent experiments and the bar indicates the SD values (*p < 0.05, **p < 0.01). GC, gastric cancer.

lncRNA-profiles characteristic of polarized macrophages. Here, 933 differentially expressed lncRNAs (709 upregulated and 224 downregulated genes, figure 1B) and 819 differentially expressed mRNAs (457 upregulated and 362 downregulated genes, figure 1C) between M0 and M2-like macrophages were identified (fold change≥2 or ≤0.5, p<0.05). To validate the microarray data, six differentially expressed and immune-related lncRNAs were selected for qPCR analysis and the data confirmed their change in expression as revealed by the microarray (figure 1D). Of those, the lncRNA NR_109861 (abbreviated as NR_109) was significantly increased in M2-like macrophages compared with both M0 and M1-like macrophages (figure 1E), especially in a time-dependent manner after IL-4 treatment for 12 hours, 24 hours and 48 hours by 5.16±0.25 fold (mean±SD), 6.12±0.30 fold and 8.04±0.58 fold, respectively (figure 1F). Moreover, the expression of NR_109 was also confirmed to be elevated in M2-like macrophages derived from PBMCs with low TNF-α expression and high CD206 and Arg-1 expression (online supplemental figure S1G and H and figure 1G). Then, we observed that NR_109 was expressed in CD206$^+$ TAMs of GC tissues (online supplemental figure S1I). Compared with the macrophages derived from the matched adjacent non-neoplastic tissues (non-GC), the expression of NR_109 was increased in macrophages isolated from primary GC tissues (pri-GC) with high expression of CD163 and CD206 (figure 1H and online supplemental figure S1J), suggesting that NR_109 might be an M2-like macrophage associated lncRNA.

To identify the role of NR_109 in macrophage polarization, we knocked down or overexpressed NR_109 in M2-like macrophages to obtain M2-NR_109^{low} or M2-NR_109^{high} macrophages, respectively (figure 1I). As shown in figure 1J and online supplemental figure S1K and L, the expression of M2-associated molecules including CD206, Arg-1, TGF-β and IL-10 was reduced in M2-NR_109^{low} cells, but enhanced in M2-NR_109^{high} macrophages, while the expression of M1-associated markers including HLA-DRα, CD206, TNF-α and IL-12 was increased in M2-NR_109^{low} cells, but decreased in M2-NR_109^{high} macrophages. Moreover, in macrophages induced from PBMC, the expression of CD206 was also downregulated in M2-NR_109^{low} cells (figure 1K). In addition, compared with the control group, the level of IL-12 and TNF-α was elevated, while the level of IL-10 and TGF-β was attenuated in the supernatant of M2-NR_109^{low} macrophages (figure 1L). Interestingly, the expression of M2 markers was reduced when knocking down NR_109 in M0 cells, suggesting that NR_109 knockdown hindered IL-4 induced M2-like macrophage polarization (figure 1M). On the other hand, compared with M0 and M1-like macrophages, the expression of M2-associated markers was elevated when forced expression of NR_109 in those cells (figure 1N). Collectively, our results demonstrated for the first time that NR_109 facilitated the generation of pro-tumor phonotype of macrophages.

Then, we performed 5′-RACE and 3′-RACE to further characterize the features of NR_109. The results determined that the full-length NR_109 is 1036 nucleotides long, which was identical to ENST00000449270 in the Ensembl database (figure 1O and online supplemental figure S1M and N) and longer than the sequence in the NCBI database (808 nt, gene ID: 101929371, results not shown). Moreover, searching the CPAT (Coding Potential Assessment Tool, https://wlcb.oit.uci.edu/cpat) and CPC 2 (Coding Potential Calculator 2, http://cpc2.gaolab.org) databases, NR_109 barely had any coding probability, suggesting that NR_109 was indeed a non-coding RNA (online supplemental figure S1O). According to NONCODE database, NR_109 expression was preferentially distributed in lymphoid organs, including the thymus and lymph nodes, as well as macrophage-enriched tissues, such as the lung and brain, suggesting a potential role for NR_109 in immune cells (online supplemental figure S1P).

Knockdown of NR_109 reduced the activity of M2-like macrophages to promote the proliferation and metastasis of cancer cells

It has been reported that M2-like macrophages promote the proliferation and metastasis of many cancer cells by providing cytokines and enzymes, such as TGF-β, IL-10, Arg-1 and IDO.[9 26–28] Our data also confirmed that the cells or the supernatant of M2-like macrophages could promote the growth and migration of cancer cells (online supplemental figure S2A–C). Then, we examined the effect of NR_109 on the function of M2-like macrophages. First, the tumor cells AGS, MDA-MB-231, BGC-823, A549 and Eca109 were cocultured with the medium containing 30% supernatant from M2-NR_109^{low} macrophages and the results showed that compared with the control group, the proliferation of tumor cells was significantly decreased after treatment with the M2-NR_109^{low} medium (figure 2A and online supplemental figure S2D). Consistently, the percentage of EdU$^+$ AGS and EdU$^+$ MBA-MD-231 cells was also reduced when cocultured with 30% supernatant of M2-NR_109^{low} (figure 2 and online supplemental figure S2E). Subsequently, a coculture model using tumor cells and M2-NR_109^{low} or M2si-NC cells were established to explore the role of macrophages on migration of tumor cells (online supplemental figure S2F). As shown in figure 2C and online supplemental figure S2G, the migration of tumor cells cocultured with M2-NR_109^{low} cells was significantly decreased compared with that of the control group. All these data indicated that M2-NR_109^{low} reduced the activity of M2-like macrophage to mediate the growth and migration of various tumor cells in vitro.

To further evaluate the function of M2-NR_109^{low} on tumor cells in vivo, NPG mice, in which T/B lymphocytes and NK cells were depleted, were transplanted with enriched CD34$^+$ HSCs isolated from fresh human umbilical cord blood to reconstitute the human immune system[29 30] (online supplemental figure S2H). By analysis,
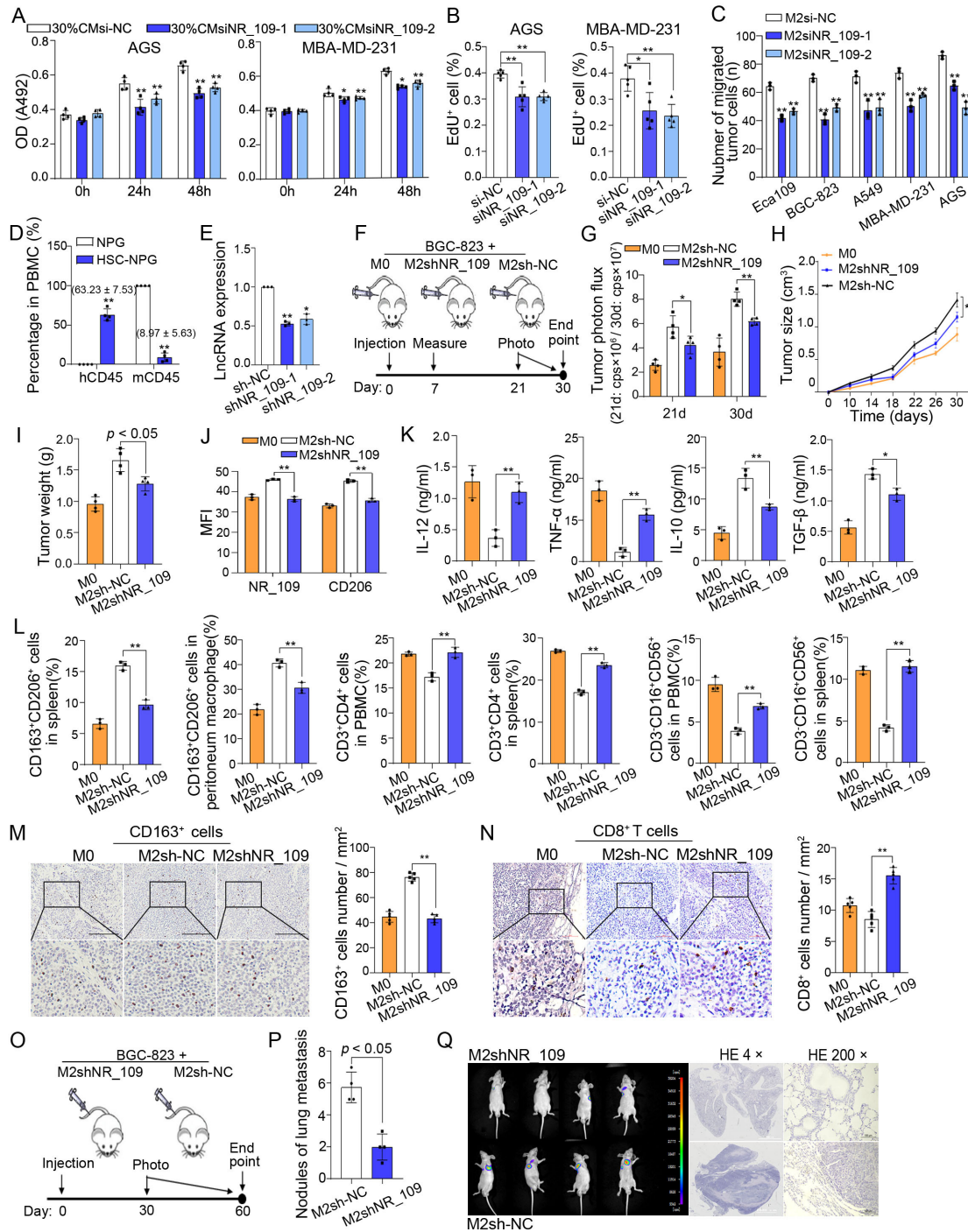
Figure 2 Knockdown of NR_109 reduced the activity of M2-like macrophages to promote growth and metastasis of cancer cells. (A) The MTS and (B) EdU incorporation assays showed the proliferation of tumor cells in the coculture system with 30% culture medium (CM) of M2-NR_109low. (C) The migration of tumor cells when cocultured with M2-NR_109low cells. (D) The proportion of hCD45+ cells in the PBMC of NPG mice and HSC-NPG mice (8.97% ± 5.63% vs. 63.23% ± 7.53%). (E) Expression of NR_109 in M2-like macrophages after NR_109 lentiviral transduction was measured by qPCR. (F) The sketch of subcutaneous xenograft model in HSC-NPG mice. (G) The tumor growth (shown as photon flux) was examined by in vivo imaging. (H) The tumor size, (I) tumor weight and (J). MFI of NR_109 and CD206 in tumor tissues of different groups were analyzed. (K) The level of IL-12, TNF-α, IL-10 and TGF-β in the serum of HSC-NPG mice from distinct groups was tested by ELISA. (L) The percentage of M2-like macrophages (CD163+CD206+) in spleen and peritoneum macrophages, and the percentage of CD4+ T cells and NK cells (CD3-CD16+CD56+) in the PBMC and spleen were measured by FCM. (M) The infiltration of CD163+ cells and N. the number of CD8+ T cells in tumor tissues of different groups was detected by using IHC assays.(O) The sketch of metastatic tumor model in nude BALB/c mice. (P) The number of lung metastasis nodules was examined. (Q) In vivo imaging and HE staining showed the lung metastasis nodules and the representative regions of the lung in HSC-NPG mice of the two groups. The statistical data are from three independent experiments and the bar indicates the SD values (*p < 0.05, **p < 0.01).)MFI, mean fluorescence intensity.

the proportion of human CD45^{+} leucocytes reached 63.23%±7.53% in total circulating CD45^{+} cells after reconstitution (figure 2D and online supplemental figure S2I). Moreover, CD3^{+} T cells, CD14^{+} cells, CD19^{+} B cells and CD56^{+} NK cells derived from human were also detected in the peripheral blood of HSC-NPG mice (online supplemental figure S2J), confirming the successful establishment of a humanized immune system in these HSC-NPG mice.

Subsequently, M2shNR_109 cells were established to have NR_109 stably knocked down in M2-like macrophages (figure 2E and S2K). Then, luciferase-expressing BGC-823 cells mixed with M2shNR_109 cells, M2sh-NC cells or M0 cells at a ratio of 3:1 were injected into the right flank of HSC-NPG mice (figure 2F). On 21 d and 30 d after inoculation, the tumor size was measured by in vivo imaging (online supplemental figure S2L). Compared with the M0 group, M2sh-NC cells facilitated the growth of tumors, while compared with M2sh-NC cells, M2shNR_109 cells partially impaired activity on tumor growth (figure 2G). Moreover, the tumor size, tumor weight and the mean fluorescence intensity of NR_109 and CD206 in tumor tissues of the M2shNR_109 group were significantly reduced compared with that of the M2sh-NC group (figure 2H–2J and S2M). Furthermore, compared with the M2sh-NC group, the level of IL-12 and TNF-α in serum was increased, while the level of IL-10 and TGF-β was significantly decreased in the serum of the M2shNR_109 group (figure 2K). In addition, the percentage of M2-like macrophages (CD163^{+}/CD206^{+}) in the spleen and peritoneum was downregulated, while the percentage of CD4^{+} T cells and NK cells (CD3^{-}CD16^{+}CD56^{+}) in the PBMC and spleen was significantly upregulated in the M2shNR_109 group compared with that of the M2sh-NC group (figure 2L and online supplemental figure S2N and P). In parallel, IHC staining assays showed that compared with the M2sh-NC group, the infiltration of CD163^{+} macrophages was reduced and the number of CD8^{+} T and CD4^{+} T cells was enhanced in the tumor tissues of the M2shNR_109 group (figure 2M,N and and online supplemental figure S3A). Since the polarization states of macrophages could affect the malignant properties of tumor cells, Ki67 and epithelia-mesenchymal-transition (EMT)-related markers were measured in tumor tissues by IHC assays.[31 32] Accordingly, compared with that of the M2sh-NC group, the Ki-67 index and the expression of N-cadherin and Vimentin was significantly decreased, whereas the expression of E-cadherin was elevated in the M2shNR_109 group (online supplemental figure S3B–D). To further elucidate the effect of NR_109 in M2-like macrophages on tumor metastasis in vivo, a mixture of luciferase-expressing BGC-823 cells and M2shNR_109 or M2sh-NC (at a ratio of 3:1) was injected into the tail veil of BALB/c nude mice (figure 2O). As shown in figure 2P,Q and online supplemental figure S3E and F, compared with the M2sh-NC group, the number of lung metastasis nodules and the tumor size (show as photon flux) in mice of the

M2shNR_109 group had significantly reduced on day 60. Collectively, these data suggested that knockdown of NR_109 in M2-like macrophages partially restored the proportion of antitumor immune cells and cytokines, and altered the tumor growth and metastasis in vivo.

NR_109 interacted with FUBP1 protein

To explore the underlying mechanism of NR_109 in M2-like macrophage polarization, we first used FISH and subcellular fractionation assays to probe the location of NR_109. The results showed that NR_109 was predominantly localized in the nucleus (figure 3AB). Previous studies have demonstrated that nucleus-located lncRNAs exerted their biological function mainly by forming complexes with proteins.[15] Therefore, we performed an RNA pull-down assay using in vitro transcribed biotinylated NR_109 to identify NR_109-interacting proteins in M2-like macrophages. As shown in figure 3C, an obvious band with a size between 55 kDa and 72 kDa was specifically enriched in the NR_109 pull-down. The specific band was analyzed by mass spectrometry and some of the potential NR_109-interacting proteins were listed in figure 3D. Then, pull down products were subjected to western blot assays and indicated that the FUBP1, which was a transcription regulator and primarily located in the nucleus, was identified as a candidate NR_109-interacting protein (figure 3E). Consistently, RIP assays further confirmed the interaction of NR_109 with FUBP1 (figure 3F). Moreover, to elucidate the binding site between NR_109 and FUBP1, a series of truncated probes were designed according to the secondary structure of NR_109 as predicted by the RNAfold WebServe database (http://rna.tbi.univie.ac.at/cgibin/RNAWeb-Suite/-RNAfold.cgi) (figure 3G). As shown in figure 3H, the 476–640 nt region of NR_109 (P3) was identified as the sequence required for direct interaction.

Subsequently, to better understand the association between the expression of FUBP1 and the infiltration of M2-like macrophages in the tumor tissues, we searched the TIMER2.0 database (http://timer.comp-genomics.org/) and revealed a significant positive correlation between the expression of FUBP1 and the infiltration of M2-like macrophages in many cancer types (online supplemental figure S3G). Then, we generated M2-FUBP1^{low} and M2-FUBP1^{high} cells with FUBP1-siRNA and FUBP1-plasmid, respectively, to investigate the function of FUBP1 in M2-like macrophage polarization (figure 3I,J). As shown in figure 3K, the expression of M2 markers, including Arg-1, CD206, IL-10, TGF-β and VEGF was markedly decreased in M2-FUBP1^{low} cells but increased in M2-FUBP1^{high} cells. To further confirm the results, M2-like macrophages were treated with the FUBP1 inhibitor, FUBP1-IN-1 for 24 hours and the expression of FUBP1 was suppressed in those cells (online supplemental figure S3H and I). Moreover, the level of M2 markers, including CD163, CD206, Arg-1, VEGF and IL-10 were also significantly decreased (24 µM, 24 hours) (online supplemental figure S3J). In addition, the migration of tumor cells
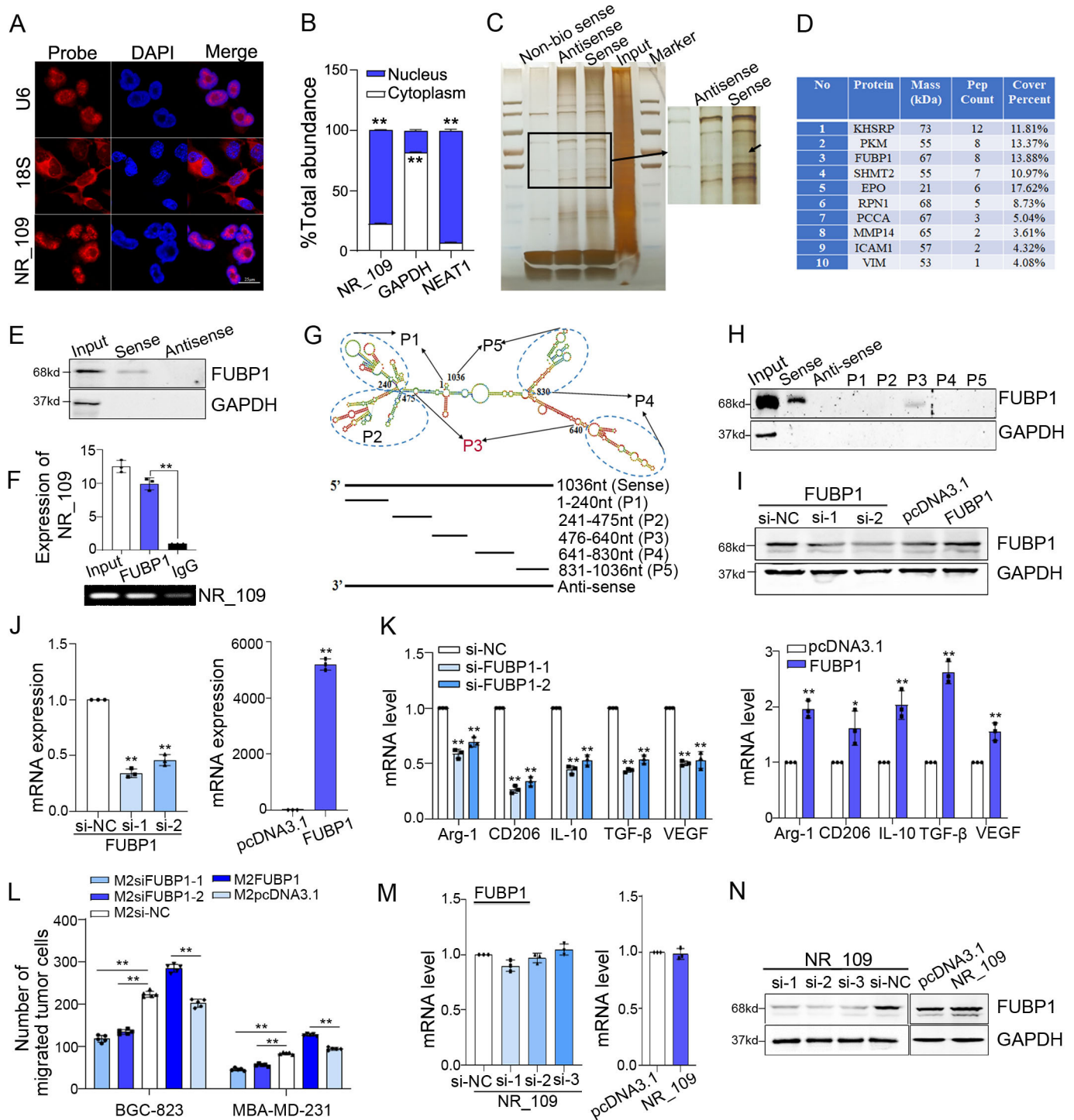
Figure 3 NR_109 interacted with FUBP1 protein. (A) FISH and (B) nuclear and cytosolic RNA analyses revealed that NR_109 was mainly located in the nucleus of M2-like macrophages. (C) The interacted proteins of NR_109 were resolved through NR_109 pulldown assay, SDS-PAGE electrophoresis and visualized by silver staining. (D) The top 10 proteins analyzed by MS were shown. (E) Only biotinylated sense probe pulled down FUBP1 in M2-like macrophages. (F) The interaction of NR_109 and FUBP1 was confirmed by RIP assays. (G) A series of truncated probes of NR_109 was designed according to the secondary structure of NR_109.(H) The FUBP1 protein was pulled down by the P3 probe (476-640nt) of NR_109. (I-J) M2-FUBP1low and M2-FUBP1high macrophages were constructed by transfecting FUBP1 siRNA or FUBP1 plasmid, respectively. (K) Expression of M2 markers and (L) the migration of tumor cells were measured by qPCR and transwell assays. (M-N) NR_109 affected FUBP1 at the protein level, but not the mRNA level. The statistical data are from three independent experiments and the bar indicates the SD values (*p < 0.05, **p < 0.01). FUBP1, far upstream element-binding protein 1.

was reduced when cocultured with M2-FUBP1^{low} cells but was enhanced when cocultured with M2-FUBP1^{high} cells (figure 3L and online supplemental figure S3K). Overall, these findings suggested that FUBP1, a NR_109-interacting protein, was an essential factor during M2-like macrophage polarization.

NR_109 blocked the ubiquitin-mediated degradation of FUBP1 by competing with JTV-1

To explore the effect of NR_109 on FUBP1 expression, both the mRNA and protein levels of FUBP1 were measured in M2-NR_109^{low} and M2-NR_109^{high} cells. As shown in figure 3M,N, the level of FUBP1 protein, but not mRNA was significantly changed. Therefore, we expected that NR_109 might interact with FUBP1 and enhance its stability. Then, to understand the mechanism by which NR_109 promoted FUBP1 protein expression, a series

of flag-tagged FUBP1 deletion mutants was designed to investigate which domain of FUBP1 was responsible for binding to NR_109 (figure 4A,B). As shown in figure 4C, we found that the C-terminus (447-644) of FUBP1 was essential for the binding of FUBP1 to NR_109 using RIP assays.

It was reported that aminoacyl tRNA synthase complex-interacting multifunctional protein 2 (JTV-1) could physically bind to the C-terminus of FUBP1 and promote FUBP1 degradation via ubiquitination.[33] Based on our previous findings, we envisioned that NR_109 might bind to the same domain to block the ubiquitin-mediated proteasomal degradation of FUBP1 by competing with JTV-1. To verify this hypothesis, we first used the protein synthesis inhibitor cycloheximide (CHX) to evaluate the effect of NR_109 on the degradation of FUBP1. As shown
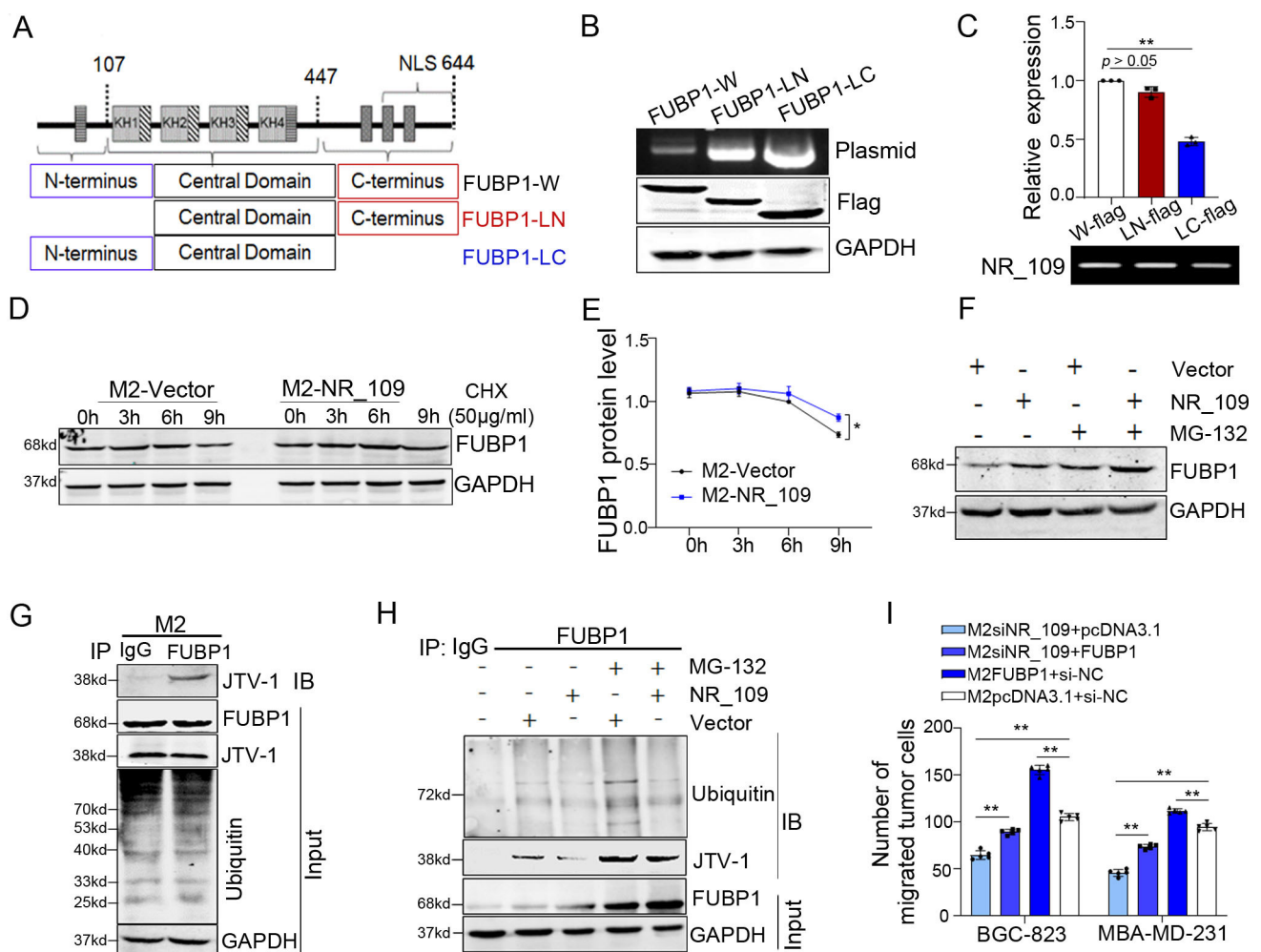

Figure 4 NR_109 inhibited the ubiquitin-mediated degradation of FUBP1. (A) The structure of FUBP1 protein. (B) The flag-tagged-FUBP1 deletion mutations. (C) RIP assays showed that loss of C-terminus of FUBP1 decreased the activity to precipitate NR_109. (D–E) Degradation of FUBP1 was reduced in NR_109- overexpressing M2-like macrophages treated with CHX. (F) Addition of proteasome inhibitor MG132 (25µM) further blocked the degradation of FUBP1 in NR_109 overexpressing M2-like macrophages. (G) The interaction between FUBP1 and JTV-1 was verified by co-IP assay. (H) Ectopic NR_109 expression decreased the density of ubiquitin and JTV-1, and the MG132 further enhanced the effect. (I) Co-transfection with FUBP1 plasmid and NR_109 siRNA in M2-like macrophages partially reversed the migration of cocultured tumor cells. FUBP1-W: whole of FUBP1, FUBP1-LC: loss C-terminus FUBP1, FUBP1-LN: loss N-terminus FUBP1. The statistical data are from three independent experiments and the bar indicates the SD values (*p < 0.05, **p < 0.01).

in figure 4D and E, overexpression of NR_109 in M2-like macrophages prolonged the half-life of FUBP1. Then, inhibiting proteasome activity with MG132 indicated the prevention of ubiquitin-mediated degradation of FUBP1 in M2-NR_109^{high} cells (figure 4F and online supplemental figure S4A). Next, the co-IP assays confirmed the interaction between FUBP1 and JTV-1 (figure 4G). Moreover, the anti-FUBP1 antibody coprecipitated with a lower density of ubiquitin and JTV-1 when ectopic NR_109 was expressed in M2-like macrophages and this function was more obvious in the presence of MG132 (figure 4H and online supplemental figure S4B). In addition, overexpression of FUBP1 partially rescued the cocultured tumor cell migration impairments caused by NR_109 knockdown in M2-like macrophages (figure 4I and online supplemental figure S4C). Taken together, these results demonstrated that NR_109 enhanced the stability and activity of FUBP1 by inhibiting its ubiquitin-mediated proteasomal degradation pathway.

FUBP1 promoted M2-like macrophage polarization by upregulating *c-Myc* transcription

It was reported that FUBP1 was a DNA-binding protein which contributed *c-Myc* gene transcriptional regulation and was first identified from undifferentiated HL60 cells.[34 35] By searching the RNA-Protein Interaction Prediction (RPISeq) website (http://pridb.gdcb.iastate.-edu//RPISeq/), we verified a high interaction probability score between FUBP1 protein and the *c-Myc* RNA sequence, indicating a close interaction between them (RF classifier: 0.8; SVM classifier: 0.95; the interaction probabilities score ranged from 0 to 1 and >0.5 were considered 'positive', online supplemental figure S5A). It was reported that c-Myc directly regulated some genes which manipulated the polarization states of macrophages, including CD206, SCARB1 and etc[36 37] and the cBioPortal database (http://www.-cbioportal.org-/public-portal/) also confirmed a positive correlation between the mRNA expression level of c-Myc and TAM markers, including CD163, CSF1R and FOLR2 in breast cancer[38 39] (online supplemental figure S5B). Furthermore, our results exhibited that, compared with that of M0 and M1-like macrophages, the expression of c-Myc was increased in M2-like macrophages (figure 5A). Similarly, the expression of FUBP1 and c-Myc was significantly evaluated in M2-like macrophages derived from PBMC (figure 5B). Therefore, it was reasonable to assume that FUBP1 might influence the M2-like macrophage polarization by regulating c-Myc. Consistent with this hypothesis, we observed that downregulation of FUBP1 reduced the expression of c-Myc, while upregulation of FUBP1 enhanced the expression of c-Myc at both the mRNA and protein levels (figure 5C,D). To verify the function of c-Myc in M2-like macrophage polarization, we established M2-c-Myc^{low} and M2-c-Myc^{high} cells by transfecting siRNA and c-Myc-plasmid, respectively (figure 5E,F). As shown in figure 5G,H, the expression

of M2 markers, including Arg-1, CD206, IL-10, TGF-β and SCARB1 was downregulated in M2-c-Myc^{low} cells but upregulated in M2-c-Myc^{high} cells. Additionally, the migration of tumor cells was evidently reduced in the coculture system of M2-c-Myc^{low}, while the opposite was observed in the coculture system of M2-c-Myc^{high} (figure 5I and online supplemental figure S5C). All these data indicated that c-Myc which was regulated by FUBP1 was an important participant of M2-like macrophage polarization.

Subsequently, we explored the expression correlation between NR_109 and c-Myc in M2-like macrophages. As shown in figure 5J, the expression of c-Myc was decreased in M2-NR_109^{low} cells but increased in M2-NR_109^{high} cells, indicating that NR_109 could regulate the expression of c-Myc. Furthermore, knocking down NR_109 reversed the c-Myc-mediated high expression of M2 markers, including CD206, IL-10 and SCARB1, as well as the migration of tumor cells in the coculture system (figure 5K,M and online supplemental figure S5M). Importantly, our data showed that overexpressing FUBP1 could partially restore the expression of c-Myc in M2-NR_109^{low} cells, suggesting that NR_109 regulated the expression of c-Myc through FUBP1 (figure 5N). In summary, these results demonstrated that NR_109 promoted M2-like macrophage polarization via the FUBP1/c-Myc axis.

NR_109/FUBP1/c-Myc was a positive feedback loop that promoted M2-like macrophage polarization

To explore the upstream drivers of NR_109, we predicted the potential transcription factors of NR_109 in the JASPAR, PROMO and UCSC databases. Interestingly, c-Myc was a potential transcription factor of NR_109, and the possible binding sequence was CACGTG (figure 6A,B). To verify the c-Myc binding site in the NR_109 promoter, we performed a ChIP assay in M2-like macrophages. The results showed that c-Myc could precipitate the promoter of NR_109 only when NR_109 harbored the c-Myc BR sequence 'CACGTG'. After the c-Myc binding site in NR_109 was deleted (NBR), c-Myc could not enrich NR_109 (figure 6C). To further confirm this result, we mutated the c-Myc binding sites in the NR_109 promoter and performed a dual-luciferase reporter assay, in which the luciferase reporter gene was driven by the NR_109 promoter. As expected, the mutant promoter was no longer activated in response to c-Myc overexpression (figure 6D). Moreover, the expression of NR_109 was significant decreased in M2c-Myc^{low} cells but increased in M2c-Myc^{high} cells (figure 6E). Accordingly, our data demonstrated that as an essential transcription factor, c-Myc could directly bind to the CACGTG sequence in the NR_109 promoter and enhance the transcription of NR_109.

Subsequently, the relationship among the expression of NR_109, FUBP1 and c-Myc was investigated in clinical tumor samples by ISH and IHC analyses. As shown in figure 6F,G, the expression of NR_109 was positively
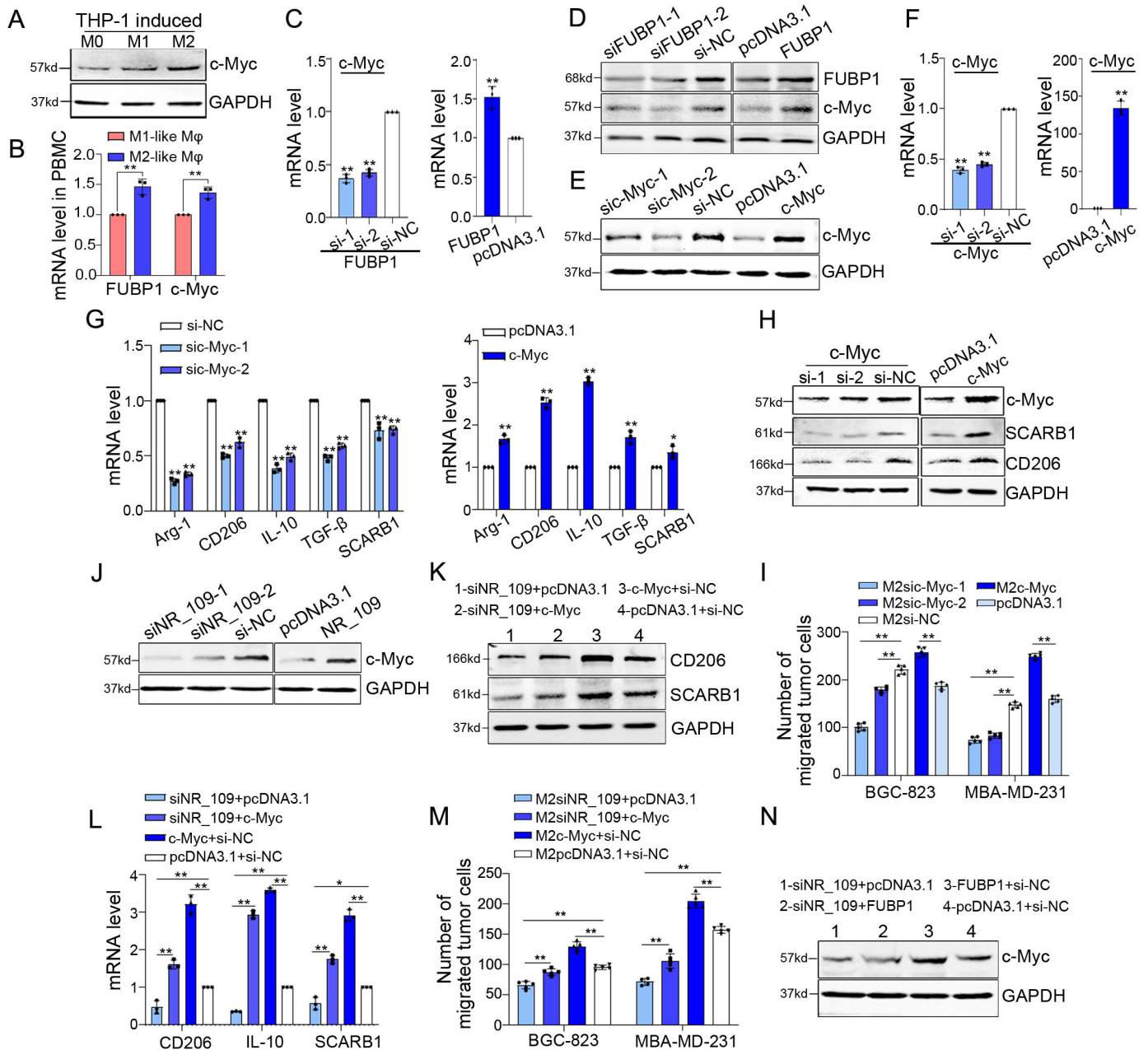
Figure 5 FUBP1 promoted M2-like macrophage polarization through c-Myc. (A) Expression of c-Myc in M0, M1 and M2-like macrophages derived from THP-1 cells was measured using western-blot assay. (B) Expression of FUBP1 and c-Myc in M2-like macrophages derived from PBMC was tested by qPCR. (C–D) The expression of c-Myc was affected by FUBP1 at both mRNA and protein levels. (E–F) M2-c-Myclow cells and M2-c-Mychigh cells were established by transfecting c-Myc siRNA or c-Myc-plasmid, respectively. (G–H) Expression of M2-related markers in M2-like macrophages with NR_109 knockdown and overexpression were measured by western-blot and qPCR assays. (I) Migration of tumor cells cocultured with M2-c-Myclow or M2-c-Mychigh cells was analyzed. (J) Expression of c-Myc in M2-NR_109low cells and M2-NR_109high cells was detected using western-blot. (K) Knockdown NR_109 reversed the c-Myc-mediated high expression of M2-related markers and M. the migration of tumor cells in the coculture system. (N) Overexpression of FUBP1 could partially restore the expression of c-Myc in NR_109low cells. The statistical data are from three independent experiments and the bar indicates the SD values (*p < 0.05, **p < 0.01). FUBP1, far upstream element-binding protein 1.

related with FUBP1 in CD68^{+} TAMs of GC (r=0.550, p=0.002) and BC (r=0.501, p=0.001). Moreover, the protein level of FUBP1 was positively related to c-Myc in CD68^{+} TAMs of GC (r=0.613, p=0.002) and BC (r=0.521, p<0.001) (figure 6H,I). Then, to define the association between NR_109 and c-Myc, we analyzed the expression of

NR_109 and c-Myc in CD68^{+} TAMs from GC, BC and lung cancer (LC) tissues by ISH and IHC assays and the representative staining regions of tissue slides with different grades of tumors are presented in online supplemental figure S6A. The colocalization analysis showed that the expression of c-Myc was positively associated with NR_109
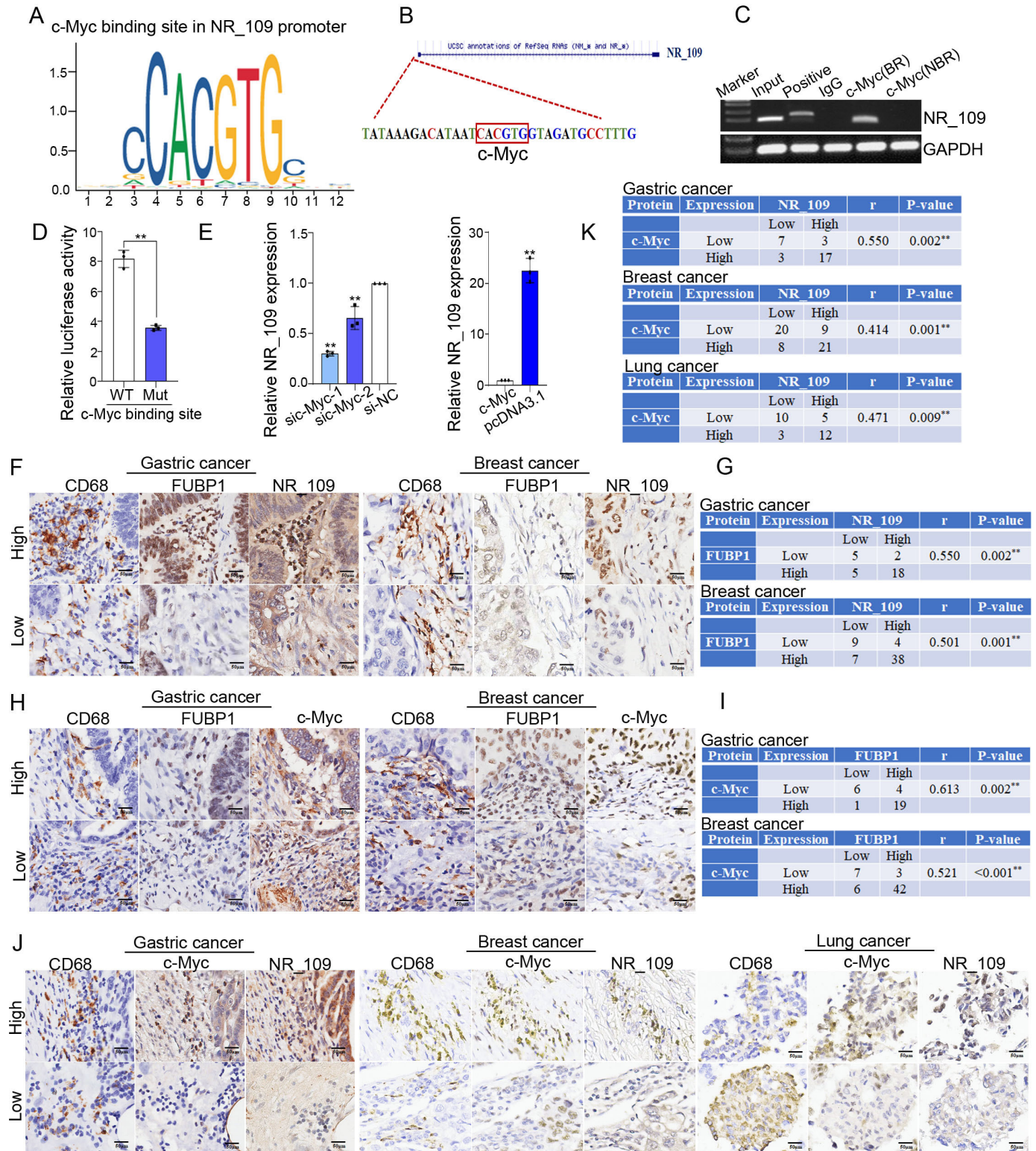
Figure 6 NR_109/FUBP1/c-Myc was a positive feedback loop to promote M2-like macrophage polarization. (A) The JASPAR and (B) PROMO database indicated that c-Myc was a potential transcription factor of NR_109 and the binding sequence was CACGTG. (C) The ChIP and (D) dual-luciferase reporter assays showed that c-Myc directly interacted with the promoter of NR_109. (E) Expression of NR_109 in M2-c-Myclow cells and M2-c-Mychigh cells was measured by qPCR. (F–G) The correlation between the expression of NR_109 and FUBP1, and (H–I) the protein level of FUBP1 and c-Myc in CD68+ TAMs of GC and BC tissues were detected using ISH and IHC assays. (J–K) The correlation between the expression of c-Myc and NR_109 in CD68+ TAMs of GC, BC and LC tissues was analyzed by ISH and IHC assays. The statistical data are from three independent experiments and the bar indicates the SD values (*p < 0.05, **p < 0.01). FUBP1, far upstream element-binding protein 1.

in CD68^{+} TAMs of GC (r=0.550, p=0.002), BC (r=0.414, p=0.001) and LC (r=0.471, p=0.009) (figure 6J,K). In summary, these results demonstrated the positive correlations among the expression of NR_109, FUBP1 and c-Myc in clinical tumor samples.

Clinical significance of NR_109 in TAMs from GC and BC

To appreciate the clinical significance of NR_109 in TAMs during cancer development, we explored the distribution of CD163^{+} TAMs and the expression of NR_109 in CD163^{+} TAMs from GC and BC tissues. As shown in figure 7A, B , CD163^{+} TAMs were presented in both tumor stromal (TS)

B

Distribution pattern of CD163^{+} TAMs in GC and BC

Variables	Mean	SE	Median	Range	P
GC					< 0.001**
TS	51.01	19.99	50.5	12-107	
TN	11.01	11.62	7	0-47	
BC					< 0.001**
TS	40.09	22.04	35	5-112	
TN	11.97	13.08	9	0-80	

**The values had statistically significant differences.
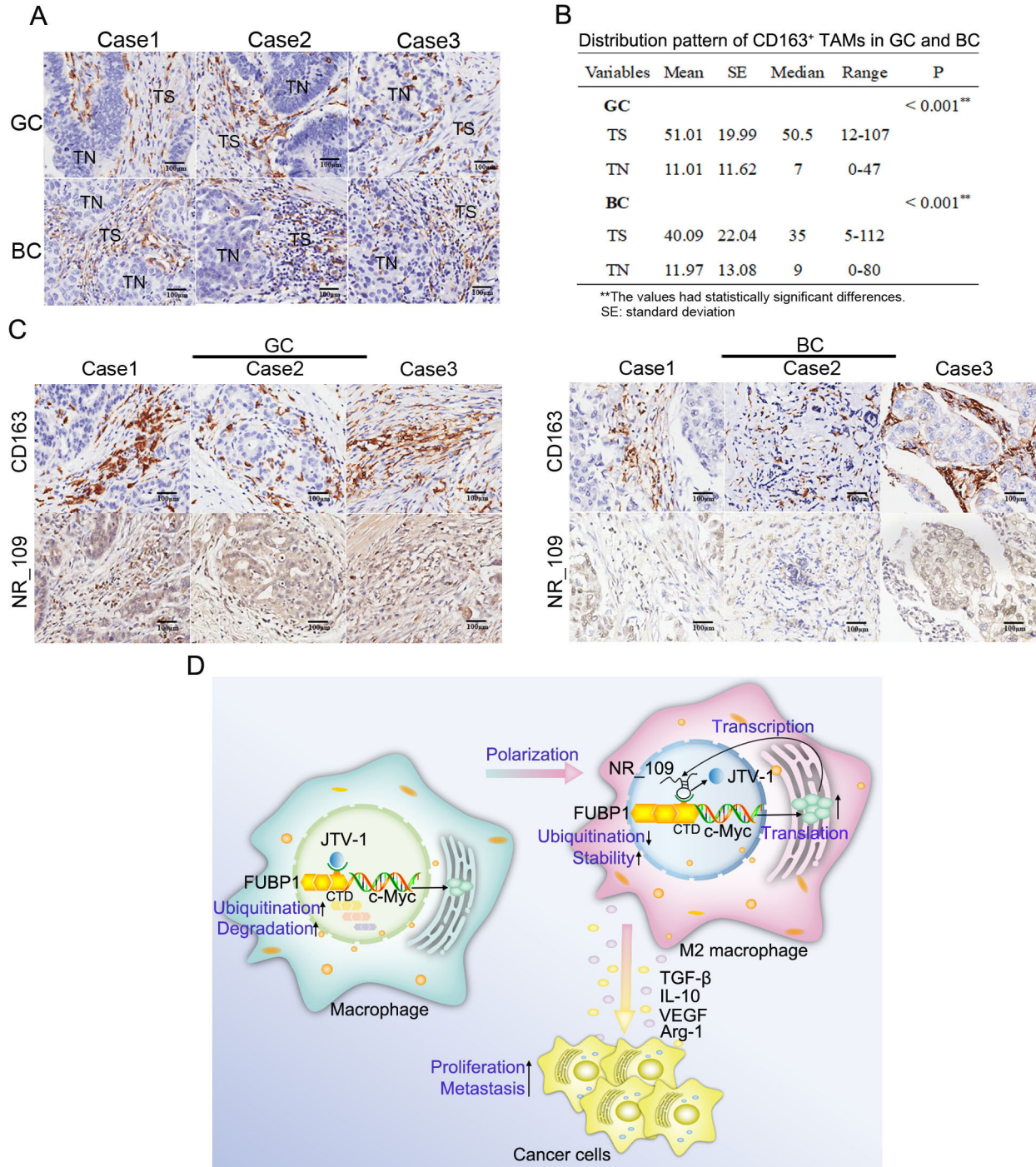SE: standard deviation

Figure 7 The clinical significance of NR_109. (A) The infiltration of CD163+ TAMs in both TS and TN was detected by IHC. (B) Statistical results indicated that there was more CD163+ TAMs infiltrated in TS than in TN (GC: 51.01 ± 19.99 vs. 11.01 ± 11.62; BC: 40.09 ± 22.04 vs. 11.97±13.08, p < 0.001). (C) In the TS, the expression of NR_109 was significantly enhanced in TAMs with more infiltrated CD163+ TAMs. (D) The graphical illustration showed how NR_109 facilitated to tumor progression by regulating the M2-like macrophage polarization. FUBP1, far upstream element-binding protein 1; TN, tumor nest; TS, tumor stroma. *p < 0.05, **p < 0.01.

and tumor nest (TN), and more CD163^{+} TAMs infiltrated in TS than that in TN (GC: 51.01±19.99 vs 11.01±11.62; BC: 40.09±22.04 vs 11.97±13.08, p<0.001). Then, the multivariate analysis showed that high CD163^{+} TAM infiltration in TS was associated with lymph node metastasis (p=0.045), while high CD163^{+} TAM infiltration in TN was related to tumor grade in GC (p=0.034). For BC, high CD163^{+} TAM infiltration in TS was associated with age (p=0.022) and TNM stage (p=0.020), while high CD163^{+} TAM infiltration in TN was related to lymph node metastasis (p=0.049) (online supplemental table S1). Moreover, the expression of NR_109 was enhanced in CD163^{+} TAMs and was positively associated with the number of CD163^{+} TAMs in the TS of both GC and BC (figure 7C and online supplemental table S2). Furthermore, analysis of the relationship between expression of NR_109 in CD163^{+} TAMs and clinicopathological features uncovered that high NR_109 expression in CD163^{+} TAMs was significantly associated with gender (p=0.024) as well as lymph node metastasis (p=0.045) in GC and TNM stages (p=0.036) in BC (table 1). Together, these results suggested that NR_109 was upregulated in CD163^{+} TAMs of patients with GC or BC and was positively related to tumor progression, revealing the important role of NR_109 in TAM-mediated cancer development.

In summary, our results demonstrated that NR_109 facilitated M2-like macrophage polarization through hampering the ubiquitin-mediated degradation of FUBP1 and further activating M2-related polarization factor c-Myc. As a transcription factor, c-Myc in turn promoted the expression of NR_109 (figure 7D). Importantly, NR_109 in TAMs was analogous to a trigger and set off an NR_109/FUBP1/c-Myc positive feedback loop to establish a TAM-mediated tumor promoting microenvironment. These findings shed light on new molecular mechanisms of M2-like macrophage polarization mediated by lncRNA NR_109 and provided new insights into developing novelty tumor immunotherapeutic strategies.

DISCUSSION

Evidence has accumulated to support a tumor-promoting role for macrophages in cancer.[40] TAMs usually possess the properties of M2-like macrophages during tumor progression and usually correlate with a higher tumor grade and shorter survival for many cancer types,[41 42] including breast cancer,[43] GC,[44 45] glioblastoma,[46] pancreatic cancer.[47] Across years of investigation, TAMs have been found to play major roles in tumor initiation, growth, metastasis, therapy resistance and TME remodeling by secreting a wide variety of cytokines, chemokines, growth factors, enzymes and metabolites.[48–50] However, the highly plastic properties of TAMs in TME during tumor development make them tempting therapeutic targets for cancer treatment. Over the years, a lot of target molecules in M2-like TAMs have emerged and applied in preclinical studies, including inhibitors or agonists for CSF1/CSF1R,[51] CD47/SIRPα,[52] PD-1/PD-L1,[53 54] and

Table 1 Correlation between the expression of NR_109 in CD163^{+} TAMs and clinicopathological characteristics in GC and BC

Parameters	Expression of NR_109 in TAMs		
GC	Low (%)	High (%)	P value
Age/year			0.694
<60	3 (30)	7 (70)	
≥60	9 (45)	11 (55)	
Gender			0.024*
Male	12 (52)	11 (48)	
Female	0 (0)	7 (100)	
Grade			0.669
I–II	10 (43)	13 (57)	
III	2 (29)	5 (71)	
Tumor size			0.711
≤5 cm	6 (46)	7 (54)	
>5 cm	6 (35)	11 (65)	
Lymph node			0.045*
No	7 (70)	3 (30)	
Yes	5 (25)	15 (75)	
TNM stage			1.000
I–II	6 (40)	9 (60)	
III–IV	6 (40)	9 (60)	
BC			
Age/year			0.882
≤70	21 (48)	23 (52)	
>70	7 (50)	7 (50)	
Grade			0.786
I–II	15 (50)	15 (50)	
III	13 (46)	15 (54)	
Tumor size			1.000
≤4 cm	25 (49)	26 (51)	
>4 cm	3 (43)	4 (57)	
Lymph node			0.754
No	17 (50)	17 (50)	
Yes	11 (46)	13 (54)	
TNM stage			0.036*
I–II	23 (58)	17 (42)	
III–IV	5 (28)	13 (72)	

The χ^2-tests were used. *The values had statistically significant differences.
*The values had statistically significant differences.
BC, breast cancer; GC, gastric cancer; TAMs, tumor-associated macrophages.

PI3Kγ.[55] While some of these modulators demonstrated robust efficacy in vitro, their activity was far less than ideal in vivo and in-depth investigation to explore the

mechanisms underlying macrophage polarization is urgently needed.

Nowadays, lncRNAs have attracted much attention for their regulatory function in macrophage polarization.[56] Cao et al found that knockdown lncRNA-MM2P blocked cytokine-driven M2 polarization and weakened tumorigenesis, tumor growth and angiogenesis.[18] Tu et al reported that lncRNA PCAT6 facilitated M2 polarization through miR-326/RohA pathway and further promoted cholangiocarcinoma progression.[57] Liang et al indicated that CRC cell-derived exosomes transported lncRNA RPPH1 into macrophages which mediated their M2 polarization, thereby in turn promoting metastasis and proliferation of CRC cells.[19] Although lncRNAs are considered as important participants in macrophage polarization, our understanding of them is still in the initial stage and requires further studies.

In our study, we first used THP-1-induced macrophage model-based microarray analysis to characterize the lncRNA profile involved in the M2-like macrophage polarization. A novel lncRNA species, NR_109, was identified to be highly expressed in M2-like macrophages derived from THP-1 cells and PBMC, and TAMs derived from tumor tissues. Then, NR_109 knockdown impeded IL-4-induced M2-type polarization. As a result, M2-associated markers and cytokines were significantly decreased in M2-NR_109^{low} cells but increased in M2-NR_109^{high} cells, suggesting a potential role for NR_109 in the regulation of macrophage polarization. Interestingly, in 2017, an independent study by another research team had shown that NR_109 was named PARAL1 and was found to have functions in adipocyte differentiation by interacting with the paraspeckle component and RBM14/NCoAA to coactivate the master adipogenic regulator PPARγ, supporting the notion that NR_109 is a functional lncRNA.[58]

A number of studies showed that TAMs were pivotal regulators in tumor proliferation, metastasis and TME remodeling.[59–61] In this work, we found that knockdown of NR_109 significantly attenuated the proliferation and metastasis of tumor cells both in vitro and in vivo. Moreover, evidence of changes in the TME included a significant increase in the percentage of NK cells, CD4$^+$ T cells and CD8$^+$ T cells in the spleen, PBMCs and tumor tissues, a decrease in the percentage of CD163$^+$/CD206$^+$ macrophages in the spleen, peritoneum and tumor tissues, an augment in the level of serum IL-12 and TNF-α, and a reduce in the level of serum IL-10 and TGF-β in HSC-NPG mice that received M2shNR_109 cells, confirming that NR_109 was an independent driver of macrophage polarization.

Mechanistically, NR_109 primarily stabilized FUBP1 and hindered the ubiquitin-mediated degradation of FUBP1 by competing with JTV-1 at the C-terminus, revealing a novelty mechanism of macrophage polarization. Interestingly, FUBP1 was identified as a DNA-binding protein that regulated c-Myc transcription.[34] Many studies also reported that c-Myc, as a controller, manipulated M2-like

macrophage polarization and promoted an immunosuppressive TME.[62 63] Consistently, our data indicated that NR_109 facilitated M2-like macrophage polarization through the FUBP1/c-Myc pathway. We further demonstrated that c-Myc bound to the promoter region of NR_109 and promoted it transcriptional activation. In addition, the positive correlation among the expression of NR_109, FUBP1 and c-Myc was confirmed in clinical cancer tissues. Here, we proposed a positive feedback loop that mediated by NR_109 to regulate M2-like macrophage polarization and discovered a novel mechanism of c-Myc on macrophage polarization.

Clinically, the expression of NR_109 was significantly enhanced in CD163$^+$ TAMs and was positively correlated to the number of CD163$^+$ TAMs in GC and BC. Moreover, high NR_109 expression in CD163$^+$ TAMs was significantly associated with lymph node metastasis in GC and TNM stages in BC. Collectively, NR_109 could be a potential prognostic indicator in the TME.

siRNA) is an effective therapeutic to regulate target gene expression in vitro and in vivo.[64 65] With the recent progress of the effective and non-immunogenic delivery system, cancer immunotherapy will be facilitated to revolutionize biomedicine and personalized medicine by modulating or compensating the expression of abnormal genes.[66] Among them, lipid nanoparticle (LNP) or exosome loaded siRNA delivery have attracted increasing attention.[67 68] In addition, other studies also uncovered that aptamers could be exploited to introduce siRNAs into target cells.[69 70] All these suggest that the delivery of siRNAs via LNP, exosome or aptamer is a promising clinical strategy for cancer prevention and therapy. Thus, the strategies of using LNP or exosome to deliver siRNA to mediate specific NR_109 knockdown in TAMs for cancer treatment warrant further investigations.

Taken together, our research revealed for the first time that NR_109 facilitated M2-like macrophage polarization by a positive feedback loop of NR_109/FUBP1/c-Myc, shedding light on cancer immunotherapy.

Conclusion

Our study not only revealed that NR_109 promoted M2-like macrophage polarization during tumor progression but also identified the positive feedback loop of NR_109/FUBP1/c-Myc as the mechanism by which NR_109 regulated the protumor TME. LncRNA NR_109 could serve as a potential diagnostic/prognostic marker for tumor immunotherapy. Furthermore, we provided a preclinical rational means for targeting NR_109 as an immunotherapeutic strategy.

Author affiliations
[1]Research Center, The Fourth Hospital of Hebei Medical University, Shijiazhuang, China
[2]Key Laboratory of Tumor Gene Diagnosis, Prevention and Therapy; Clinical Oncology Research Center, Hebei Province, The Fourth Hospital of Hebei Medical University, Shijiazhuang, China
[3]Department of Pathology and Laboratory Medicine, University of Pennsylvania Perelman School of Medicine, Philadelphia, Pennsylvania, USA

[4]Department of Hebei Key Laboratory of Medical-industrial Integration Precision Medicine, Affiliated Hospital, North China University of Science and Technology, Tangshan, China

Competing interests All authors claim that there is no any competing interests.

Patient consent for publication Consent obtained directly from patient(s).

Ethics approval Informed consent for the use of the samples was obtained from all patients, and approval was obtained from the ethics committee of the hospital (approval number: 2019054).

Provenance and peer review Not commissioned; externally peer reviewed.

Data availability statement Data are available on reasonable request. All data relevant to the study are included in the article or uploaded as online supplemental information.

Supplemental material This content has been supplied by the author(s). It has not been vetted by BMJ Publishing Group Limited (BMJ) and may not have been peer-reviewed. Any opinions or recommendations discussed are solely those of the author(s) and are not endorsed by BMJ. BMJ disclaims all liability and responsibility arising from any reliance placed on the content. Where the content includes any translated material, BMJ does not warrant the accuracy and reliability of the translations (including but not limited to local regulations, clinical guidelines, terminology, drug names and drug dosages), and is not responsible for any error and/or omissions arising from translation and adaptation or otherwise.

ORCID iD
Cong Zhang http://orcid.org/0000-0003-2736-988X

REFERENCES

1 Casey SC, Amedei A, Aquilano K, *et al*. Cancer prevention and therapy through the modulation of the tumor microenvironment. *Semin Cancer Biol* 2015;35:S199–223.
2 Binnewies M, Roberts EW, Kersten K, *et al*. Understanding the tumor immune microenvironment (time) for effective therapy. *Nat Med* 2018;24:541–50.
3 Malfitano AM, Pisanti S, Napolitano F, *et al*. Tumor-Associated macrophage status in cancer treatment. *Cancers (Basel)* 2020;12:1987.
4 Pittet MJ, Michielin O, Migliorini D. Author correction: clinical relevance of tumour-associated macrophages. *Nat Rev Clin Oncol* 2022;19:424.
5 Christofides A, Strauss L, Yeo A, *et al*. The complex role of tumor-infiltrating macrophages. *Nat Immunol* 2022;23:1148–56.
6 Hinshaw DC, Shevde LA. The tumor microenvironment innately modulates cancer progression. *Cancer Res* 2019;79:4557–66.
7 Duan Z, Luo Y. Targeting macrophages in cancer immunotherapy. *Signal Transduct Target Ther* 2021;6:127.
8 Weng Y-S, Tseng H-Y, Chen Y-A, *et al*. MCT-1/miR-34a/IL-6/IL-6R signaling axis promotes EMT progression, cancer stemness and M2 macrophage polarization in triple-negative breast cancer. *Mol Cancer* 2019;18:42.
9 DeNardo DG, Ruffell B. Macrophages as regulators of tumour immunity and immunotherapy. *Nat Rev Immunol* 2019;19:369–82.
10 Zhang Y, Yu G, Chu H, *et al*. Macrophage-Associated PGK1 phosphorylation promotes aerobic glycolysis and tumorigenesis. *Molecular Cell* 2018;71:201–15.
11 Xiang X, Wang J, Lu D, *et al*. Targeting tumor-associated macrophages to synergize tumor immunotherapy. *Signal Transduct Target Ther* 2021;6:75.
12 Locati M, Curtale G, Mantovani A. Diversity, mechanisms, and significance of macrophage plasticity. *Annu Rev Pathol* 2020;15:123–47.
13 Caronni N, Montaldo E, Mezzanzanica L, *et al*. Determinants, mechanisms, and functional outcomes of myeloid cell diversity in cancer. *Immunol Rev* 2021;300:220–36.
14 Ransohoff JD, Wei Y, Khavari PA. The functions and unique features of long intergenic non-coding RNA. *Nat Rev Mol Cell Biol* 2018;19:143–57.
15 Statello L, Guo C-J, Chen L-L, *et al*. Author correction: gene regulation by long non-coding RNAs and its biological functions. *Nat Rev Mol Cell Biol* 2021;22:159.
16 Wang J, Zhang X, Chen W, *et al*. Regulatory roles of long noncoding RNAs implicated in cancer hallmarks. *Int J Cancer* 2020;146:906–16.
17 Herman AB, Tsitsipatis D, Gorospe M. Integrated lncRNA function upon genomic and epigenomic regulation. *Mol Cell* 2022;82:2252–66.
18 Cao J, Dong R, Jiang L, *et al*. LncRNA-MM2P identified as a modulator of macrophage M2 Polarization. *Cancer Immunol Res* 2019;7:292–305.
19 Liang Z-X, Liu H-S, Wang F-W, *et al*. Lncrna rpph1 promotes colorectal cancer metastasis by interacting with Tubb3 and by promoting exosomes-mediated macrophage M2 polarization. *Cell Death Dis* 2019;10:829.
20 Jiang P, Li X. Regulatory mechanism of lncRNAs in M1/M2 macrophages polarization in the diseases of different etiology. *Front Immunol* 2022;13:835932.
21 Green ID, Pinello N, Song R, *et al*. Macrophage development and activation involve coordinated intron retention in key inflammatory regulators. *Nucleic Acids Res* 2020;48:6513–29.
22 Floberg JM, Zhang J, Muhammad N, *et al*. Standardized uptake value for 18F-fluorodeoxyglucose is a marker of inflammatory state and immune infiltrate in cervical cancer. *Clin Cancer Res* 2021;27:4245–55.
23 Xiao H, Guo Y, Li B, *et al*. M2-Like tumor-associated macrophage-targeted codelivery of STAT6 inhibitor and IKKβ siRNA induces M2-to-M1 repolarization for cancer immunotherapy with low immune side effects. *ACS Cent Sci* 2020;6:1208–22.
24 Li Y, Zhao L, Shi B, *et al*. Functions of miR-146a and miR-222 in tumor-associated macrophages in breast cancer. *Sci Rep* 2015;5:18648.
25 Xu M, Li Y, Wang X, *et al*. Role of Hepatocyte- and macrophage-specific PPARγ in hepatotoxicity induced by Diethylhexyl phthalate in mice. *Environ Health Perspect* 2022;130:17005.
26 Taniguchi S, Elhance A, Van Duzer A, *et al*. Tumor-Initiating cells establish an il-33-tgf-β niche signaling loop to promote cancer progression. *Science* 2020;369:eaay1813.
27 Batlle E, Massagué J. Transforming growth factor-β signaling in immunity and cancer. *Immunity* 2019;50:924–40.
28 Guc E, Pollard JW. Redefining macrophage and neutrophil biology in the metastatic cascade. *Immunity* 2021;54:885–902.
29 Zhao H, Wang C, Yang Y, *et al*. ImmunoPET imaging of human CD8+ T cells with novel 68ga-labeled nanobody companion diagnostic agents. *J Nanobiotechnology* 2021;19.
30 Wang J, Li C, He K, *et al*. Characterization of anti-cd79b/CD3 bispecific antibody, a potential therapy for B cell malignancies. *Cancer Immunol Immunother* 2023;72:493–507.
31 Li W, Zhang X, Wu F, *et al*. Gastric cancer-derived mesenchymal stromal cells trigger M2 macrophage polarization that promotes metastasis and EMT in gastric cancer. *Cell Death Dis* 2019;10:918.
32 Wu J, Gao W, Tang Q, *et al*. Retracted: M2 macrophage–derived exosomes facilitate HCC metastasis by transferring αMβ2 integrin to tumor cells. *Hepatology* 2021;73:1365–80.
33 Zhang J, Chen QM. Far upstream element binding protein 1: a commander of transcription, translation and beyond. *Oncogene* 2013;32:2907–16.
34 Braddock DT, Louis JM, Baber JL, *et al*. Structure and dynamics of KH domains from FBP bound to single-stranded DNA. *Nature* 2002;415:1051–6.

35 Cukier CD, Hollingworth D, Martin SR, *et al*. Molecular basis of FIR-mediated c-myc transcriptional control. *Nat Struct Mol Biol* 2010;17:1058–64.

36 Fang DD, Tang Q, Kong Y, *et al*. Mdm2 inhibitor apg-115 synergizes with PD-1 blockade through enhancing antitumor immunity in the tumor microenvironment. *J Immunother Cancer* 2019;7:327.

37 Pello OM, De Pizzol M, Mirolo M, *et al*. Role of c-MYC in alternative activation of human macrophages and tumor-associated macrophage biology. *Blood* 2012;119:411–21.

38 Mantovani A, Marchesi F, Malesci A, *et al*. Tumour-associated macrophages as treatment targets in oncology. *Nat Rev Clin Oncol* 2017;14:399–416.

39 Samaniego R, Domínguez-Soto Á, Ratnam M, *et al*. Folate receptor β (FRβ) expression in tissue-resident and tumor-associated macrophages associates with and depends on the expression of PU.1. *Cells* 2020;9:1445.

40 Cheng K, Cai N, Zhu J. n.d. Tumor-associated macrophages in liver cancer: from mechanisms to therapy. *Cancer Commun*

41 Pathria P, Louis TL, Varner JA. Targeting tumor-associated macrophages in cancer. *Trends Immunol* 2019;40:310–27.

42 Shapouri-Moghaddam A, Mohammadian S, Vazini H, *et al*. Macrophage plasticity, polarization, and function in health and disease. *J Cell Physiol* 2018;233:6425–40.

43 Tiainen S, Tumelius R, Rilla K, *et al*. High numbers of macrophages, especially M2-like (CD163-positive), correlate with hyaluronan accumulation and poor outcome in breast cancer. *Histopathology* 2015;66:873–83.

44 Zhang H, Li R, Cao Y, *et al*. Poor clinical outcomes and immunoevasive contexture in intratumoral IL-10-producing macrophages enriched gastric cancer patients. *Ann Surg* 2022;275:e626–35.

45 Piao H, Fu L, Wang Y, *et al*. A positive feedback loop between gastric cancer cells and tumor-associated macrophage induces malignancy progression. *J Exp Clin Cancer Res* 2022;41:174.

46 Sørensen MD, Dahlrot RH, Boldt HB, *et al*. Tumour-Associated microglia/macrophages predict poor prognosis in high-grade gliomas and correlate with an aggressive tumour subtype. *Neuropathol Appl Neurobiol* 2018;44:185–206.

47 Atanasov G, Pötner C, Aust G, *et al*. TIE2-expressing monocytes and M2-polarized macrophages impact survival and correlate with angiogenesis in adenocarcinoma of the pancreas. *Oncotarget* 2018;9:29715–26.

48 Su S, Liu Q, Chen J, *et al*. A positive feedback loop between mesenchymal-like cancer cells and macrophages is essential to breast cancer metastasis. *Cancer Cell* 2014;25:605–20.

49 Zhang J, Muri J, Fitzgerald G, *et al*. Endothelial lactate controls muscle regeneration from ischemia by inducing M2-like macrophage polarization. *Cell Metabolism* 2020;31:1136–53.

50 Peranzoni E, Lemoine J, Vimeux L, *et al*. Macrophages impede CD8 T cells from reaching tumor cells and limit the efficacy of anti–PD-1 treatment. *Proc Natl Acad Sci U S A* 2018;115:E4041–50.

51 Salvagno C, Ciampricotti M, Tuit S, *et al*. Therapeutic targeting of macrophages enhances chemotherapy efficacy by unleashing type I interferon response. *Nat Cell Biol* 2019;21:511–21.

52 Morrissey MA, Kern N, Vale RD. Cd47 ligation repositions the inhibitory receptor SIRPa to suppress integrin activation and phagocytosis. *Immunity* 2020;53:290–302.

53 Gordon SR, Maute RL, Dulken BW, *et al*. Pd-1 expression by tumour-associated macrophages inhibits phagocytosis and tumour immunity. *Nature* 2017;545:495–9.

54 Zhu Z, Zhang H, Chen B, *et al*. PD-L1-mediated immunosuppression in glioblastoma is associated with the infiltration and M2-polarization of tumor-associated macrophages. *Front Immunol* 2020;11:588552.

55 Kaneda MM, Messer KS, Ralainirina N, *et al*. Corrigendum: PI3Kγ is a molecular switch that controls immune suppression. *Nature* 2017;542:124.

56 Mohapatra S, Pioppini C, Ozpolat B, *et al*. Non-coding RNAs regulation of macrophage polarization in cancer. *Mol Cancer* 2021;20:24.

57 Tu J, Wu F, Chen L, *et al*. Long non-coding RNA PCAT6 induces M2 polarization of macrophages in cholangiocarcinoma *via* modulating miR-326 and RhoA-Rock signaling pathway. *Front Oncol* 2020;10:605877.

58 Firmin FF, Oger F, Gheeraert C, *et al*. The RBM14/CoAA-interacting, long intergenic non-coding RNA Paral1 regulates adipogenesis and coactivates the nuclear receptor PPARgamma. *Sci Rep* 2017;7:14087.

59 Rodriguez-Garcia A, Lynn RC, Poussin M, *et al*. CAR-T cell-mediated depletion of immunosuppressive tumor-associated macrophages promotes endogenous antitumor immunity and augments adoptive immunotherapy. *Nat Commun* 2021;12:877.

60 Zhang F, Parayath NN, Ene CI, *et al*. Genetic programming of macrophages to perform anti-tumor functions using targeted mRNA nanocarriers. *Nat Commun* 2019;10:3974.

61 Cassetta L, Pollard JW. A timeline of tumour-associated macrophage biology. *Nat Rev Cancer* 2023;23:238–57.

62 Schmid MC, Khan SQ, Kaneda MM, *et al*. Integrin CD11b activation drives anti-tumor innate immunity. *Nat Commun* 2018;9:5379.

63 Esser AK, Ross MH, Fontana F, *et al*. Nanotherapy delivery of c-myc inhibitor targets protumor macrophages and preserves antitumor macrophages in breast cancer. *Theranostics* 2020;10:7510–26.

64 Tang Y, Zeng Z, He X, *et al*. Sirna crosslinked nanoparticles for the treatment of inflammation-induced liver injury. *Adv Sci (Weinh)* 2017;4:1600228.

65 Xue C, Hu S, Gao Z-H, *et al*. Programmably tiling rigidified DNA brick on gold nanoparticle as multi-functional shell for cancer-targeted delivery of siRNAs. *Nat Commun* 2021;12:2928.

66 Munagala R, Aqil F, Jeyabalan J, *et al*. Exosome-mediated delivery of RNA and DNA for gene therapy. *Cancer Lett* 2021;505:58–72.

67 Ehexige E, Bao M, Bazarjav P, *et al*. Silencing of STAT3 via peptidomimetic LNP-mediated systemic delivery of RNAi downregulates PD-L1 and inhibits melanoma growth. *Biomolecules* 2020;10:285.

68 Zhao L, Gu C, Gan Y, *et al*. Exosome-Mediated siRNA delivery to suppress postoperative breast cancer metastasis. *J Control Release* 2020;318:1–15.

69 Lv H, Wang T, Ma F, *et al*. Aptamer-functionalized targeted siRNA delivery system for tumor immunotherapy. *Biomed Mater* 2022;17:24108.

70 Herrmann A, Priceman SJ, Swiderski P, *et al*. Ctla4 aptamer delivers STAT3 siRNA to tumor-associated and malignant T cells. *J Clin Invest* 2015;125:82555.